Journal of General Virology (2014), 95, 2769–2777 DOI 10.1099/vir.0.069336-0

Human herpesvirus 6 gM/gN complex interacts with v-SNARE in infected cells

Akiko Kawabata,[1] Satoshi Serada,[2] Tetsuji Naka[2] and Yasuko Mori[1]

Correspondence
Yasuko Mori
ymori@med.kobe-u.ac.jp

[1]Division of Clinical Virology, Center for Infectious Diseases, Kobe University Graduate School of Medicine, 7-5-1, Kusunoki-cho, Chuo-ku, Kobe 650-0017, Japan

[2]Laboratory of Immune Signal, Division of Biomedical Research, National Institute of Biomedical Innovation, 7-6-8, Saito-Asagi, Ibaraki, Osaka 567-0085, Japan

Human herpesvirus 6 (HHV-6) glycoprotein M (gM) is an envelope glycoprotein that associates with glycoprotein N (gN), forming the gM/gN protein complex, in a similar manner to the other herpesviruses. Liquid chromatography-MS/MS analysis showed that the HHV-6 gM/gN complex interacts with the v-SNARE protein, vesicle-associated membrane protein 3 (VAMP3). VAMP3 colocalized with the gM/gN complex at the *trans*-Golgi network and other compartments, possibly the late endosome in HHV-6-infected cells, and its expression gradually increased during the late phase of virus infection. Finally, VAMP3 was incorporated into mature virions and may be transported with the gM/gN complex.

Received 23 June 2014
Accepted 9 September 2014

INTRODUCTION

Human herpesvirus 6 (HHV-6) belongs to the betaherpesvirus subfamily (Roizmann *et al.*, 1992). HHV-6 isolates can be classified as HHV-6A and HHV-6B (Ablashi *et al.*, 2013) based on genetic and antigenic differences, cell tropism, and pathogenesis (Ablashi *et al.*, 1991; Aubin *et al.*, 1991; Campadelli-Fiume *et al.*, 1993; Chandran *et al.*, 1992; Mori, 2009; Yamanishi *et al.*, 1988).

Herpesviruses encode several glycoproteins on the envelope of viral particles that work for entry, assembly and egress of the virus. Of these, glycoprotein M (gM) is a remarkable envelope glycoprotein as it is conserved among all herpesvirus subfamilies. Most herpesviruses, including herpes simplex virus type-1 (Baines & Roizman, 1991), pseudorabies virus (Dijkstra *et al.*, 1996) and equine herpesvirus 1 (Osterrieder *et al.*, 1996), do not require gM for replication. Marek's disease virus (Tischer *et al.*, 2002) and varicella-zoster virus (Yamagishi *et al.*, 2008) abolish virus growth *in vitro*. However, the gM protein of human cytomegalovirus (HCMV), which belongs to the betaherpesvirus subfamily, is essential for the production of infectious virus (Hobom *et al.*, 2000).

HHV-6 gM is a product of the U72 ORF and comprises 343 aa (Kawabata *et al.*, 2012; Lawrence *et al.*, 1995). Post-infection (p.i.), it is translated into a 47–63 kDa protein that is post-translationally glycosylated (Kawabata *et al.*, 2012). It is a type III transmembrane protein with seven membrane-spanning domains and a C-terminal cytoplasmic tail. HHV-6 gM interacts with the product of the U46 ORF, known as gN, to form a complex for transport to the *trans*-Golgi network (TGN) and endosomal compartments (Kawabata *et al.*, 2012). Finally, the gM/gN complex is incorporated into mature virions. Interestingly, unlike in alpha herpesviruses, HHV-6 gM is essential for virus growth (Kawabata *et al.*, 2012).

To further examine the role of HHV-6A gM during HHV-6 infection, we performed liquid chromatography (LC)-MS/MS analysis to identify the cellular components that interact with the gM/gN complex. The results showed that the gM/gN complex interacts with VAMP3 (vesicle-associated membrane protein 3).

VAMP3 is a v-SNARE (soluble *N*-ethylmaleimide-sensitive factor attachment protein receptor) protein that resides in recycling endosomes and endosome-derived transport vesicles. v-SNARE interacts with SNARE proteins on target membranes (t-SNAREs) to form *trans*-SNARE complexes, which draw the two membranes together and drive membrane fusion (Jahn & Scheller, 2006; Jahn *et al.*, 2003; Rothman, 1994; Söllner *et al.*, 1993). SNAREs are cytoplasmic-oriented type I membrane proteins that play a role in intracellular trafficking mechanisms during exocytosis by forming a complex that facilitates the transient fusion of the vesicular and plasma membrane lipid bilayers (Mohrmann & Sørensen, 2012). This membrane fusion is dependent on the formation of a complex between t-SNARE and v-SNARE proteins (Jahn & Scheller, 2006; Jahn *et al.*, 2003).

VAMP3 is localized to recycling endosomes (McMahon *et al.*, 1993) and plays a role in the fusion of recycling endosomes and the plasma membrane by forming a complex with the surface t-SNARE complex, Stx4/SNAP23 (Hu *et al.*, 2007). The VAMP3/Stx4/SNAP23 SNARE complex mediates the long-loop recycling pathway that delivers recycling endosomes and their cargo to the cell surface, and plays an important role in regulating the ability of macrophages to effectively adhere and spread on fibronectin (Veale *et al.*, 2011). VAMP3 is also involved in integrin trafficking, cell migration and cell adhesion (Luftman *et al.*, 2009; Tayeb *et al.*, 2005). In addition, it plays a role in the exocytosis of α-granules in platelets (Polgár *et al.*, 2002), as well as in the recycling of endocytosed transferrin receptors to the cell surface (Galli *et al.*, 1994).

Here, we describe the interaction between the gM/gN complex and VAMP3 in HHV-6A-infected cells and discuss the potential for the association between the gM/gN complex and VAMP3 to modify its localization and mediate its incorporation into mature virions.

RESULTS

Identification of cellular proteins interacting with the gM/gN complex

A recent study showed that the cytoplasmic tail of HCMV gM interacts with the cellular protein FIP4, which is a Rab11-GTPase effector protein important for gM/gN trafficking and for accumulation of the envelope glycoprotein complex in the assembly compartment in HCMV-infected cells (Krzyzaniak *et al.*, 2009). To examine the function of HHV-6A gM/gN, we tried to identify the cellular protein(s) that interact with the gM/gN complex. First, gM and gN were cotransfected into 293T cells and gM was immunoprecipitated from the lysates with an anti-gM mAb. Silver staining of gels containing proteins separated from the lysates of the gM/gN-expressing cells revealed several specific bands at approximately 10 kDa; these proteins were not present in the lysates of cells expressing gM alone. One specific band (Fig. 1a, arrowhead) was excised from the gel and subjected to LC-MS/MS analysis. The results of this analysis identified VAMP3 as the interacting protein (Fig. 1b).

To confirm the interaction between VAMP3 and gM/gN, lysates from cells expressing both HA-tagged gM and FLAG-tagged gN were immunoprecipitated with an anti-HA antibody, followed by Western blotting with anti-gM, anti-FLAG or anti-VAMP3 antibodies. As shown in Fig. 1c, VAMP3 was coprecipitated when gM and gN were coexpressed. However, VAMP3 was not coprecipitated when gM or gN was expressed alone. CD63 was not coprecipitated even when gM and gN were coexpressed (Fig. 1c). These results indicate that VAMP3 interacts with the gM/gN complex.

Interaction between gM and VAMP3 in HHV-6A-infected cells

To confirm the interaction between the gM/gN complex and VAMP3 in HHV-6A-infected cells, lysates from HHV-6A-infected HSB-2 cells were immunoprecipitated with an anti-gM mAb or an anti-VAMP3 antibody, followed by Western blotting with anti-gM, anti-VAMP3, anti-CD63 or anti-gB antibodies (Fig. 2). Endogenous VAMP3 coprecipitated with gM and vice versa; gB or endogenous CD63 coprecipitated with neither gM nor VAMP3 (Fig. 2b). These results indicate that gM also interacts with VAMP3 in HHV-6A-infected cells. Interestingly, although gM with a molecular mass of 15 kDa was detected in the lysates of HHV-6A-infected cells, it did not coprecipitate with the anti-VAMP3 antibody.

To examine the cellular localization of gM and VAMP3 in HHV-6A-infected cells, an indirect immunofluorescence assay (IFA) was performed using HHV-6A-infected HSB-2 cells at 96 h p.i. (Fig. 3). Confocal microscopy of HHV-6A-infected HSB-2 cells showed that gM and VAMP3 appear to partially colocalize to the same cellular compartment. In addition, gM and VAMP3 partially colocalized with TGN46, a marker of the TGN (Fig. 3b), and with CD63, a marker of late endosomes and multivesicular bodies (MVB) (Fig. 3a). The expression of endogenous VAMP3 was much lower in uninfected cells than infected cells [Fig. 3a(ii), b(ii)]. These results indicate that VAMP3 may localize with gM to the endosomal compartment in addition to TGN during the late stage of infection. Preimmune serum of guinea pig did not react with either HHV-6A-infected [Fig. 3d(i)] or uninfected cells [Fig. 3d(ii)], although anti-VAMP3 antibody obtained from the same guinea pig reacted with HHV-6A-infected cells [Fig. 3c(i)] but not uninfected cells [Fig. 3c(ii)].

VAMP3 is present in purified HHV-6A virions

Recently, we showed that HHV-6A virions are released through MVBs via the cellular exosomal pathway and that gB and gM are present on exosomes (Mori *et al.*, 2008). To examine whether VAMP3 expressed in HHV-6A-infected cells is present on virions and exosomes, we purified virions from the culture medium of HHV-6A-infected cells. As expected, VAMP3, gM and CD63 were detected by western blotting of the virion fractions (Fig. 4a). Virion fractions were confirmed with the presence of gB (Fig. 4a) and viral DNA (Fig. 4b). In addition, VAMP3 was detected on HHV-6A virions by immunogold labelling electron microscopy analysis [Fig. 4c(i)], but it was rarely detected on virions without primary antibody [Fig. 4c(ii)]. These results indicate that VAMP3 is incorporated into viral particles along with the gM/gN complex.

Intracellular localization of the gM/gN complex and VAMP3 in cells transiently expressing gM/gN

We next examined the intracellular localization of gM, gN and VAMP3 (Fig. 5). When plasmids expressing gM and gN were cotransfected into HeLa cells [Fig. 5a(i)], gM/gN colocalized with endogenous VAMP3 in the perinuclear region. However, when gM was expressed alone, it failed to colocalize with VAMP3 [Fig. 5a(ii)]. Because the gM/gN complex localized to the TGN in HHV-6A-infected cells, we hypothesized that the gM/gN complex would interact with

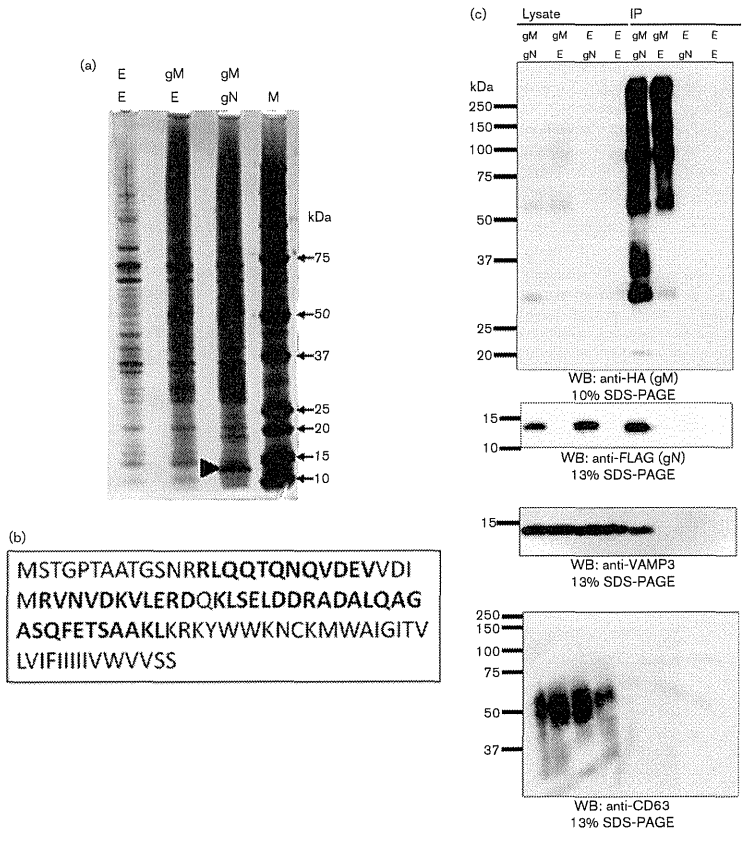

Fig. 1. Interaction between gM/gN and VAMP3. (a) 293T cells were transfected with plasmids expressing HA-tagged gM and FLAG-tagged gN. The cells were lysed with TNE buffer at 72 h post-transfection. The lysates were then immunoprecipitated with an anti-HA Ab specific for gM and visualized by silver staining. The band marked by the arrowhead indicates the protein selected for analysis by LC-MS/MS. (b) Peptide matches to the VAMP3 sequence are shown in bold. (c) 293T cells were transfected with plasmids expressing HA-tagged gM, FLAG-tagged gN, or pCAGGS (negative control). The cells were then lysed with TNE buffer at 72 h post-transfection. The lysates were immunoprecipitated with anti-HA antibody for gM and analysed by Western blotting with anti-HA, anti-FLAG, anti-VAMP3 (BioReagents) or anti-CD63 antibodies. The numbers beside the panels indicate the molecular masses (kDa). WB, Western blotting; E, empty.

VAMP3 at the TGN or a TGN-derived compartment. As expected, when gM was coexpressed with gN, it colocalized with VAMP3 and TGN46 (Fig. 5b); however, this colocalization was not observed when gM was expressed alone [Fig. 5a(ii)]. These results suggest that the interaction between the gM/gN complex and VAMP3 occurs at the TGN or a TGN-derived compartment. Glycoprotein M did not colocalize with CD63 even when gM was coexpressed with gN [Fig. 4c(i)]. Non-specific staining of gM was not seen in these cells [Fig. 5a(iii), b(ii), c(ii)].

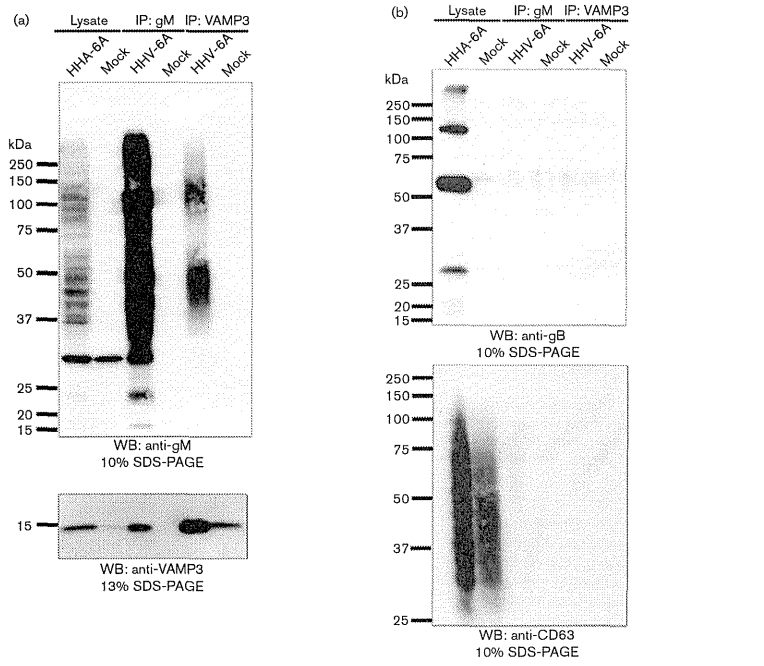

Fig. 2. Interaction between gM and VAMP3 in HHV-6A-infected HSB-2 cells. HHV-6A-infected or mock-infected HSB-2 cells were lysed with TNE buffer at 96 h post-infection. The lysates were immunoprecipitated (IP) with anti-gM mAb or anti-VAMP3 Ab (see Methods) and analysed by Western blotting with anti-gM or anti-VAMP3 (BioReagents) Abs (a), anti-gB Ab or anti-CD63 mAb (b). The numbers beside the panels indicate the molecular masses (kDa). WB, Western blotting.

The kinetics of VAMP3 expression in HHV-6A-infected cells

As shown in Fig. 2, VAMP3 expression in HHV-6A-infected cells was higher than that in mock-infected cells. Therefore, we examined the kinetics of VAMP3 expression in HHV-6A-infected cells. The results in Fig. 6 show that VAMP3 expression increased gradually in the infected cells.

DISCUSSION

Here, we used the transient expression of gM and gN to identify VAMP3 as a cellular molecule that interacts with the HHV-6A gM/gN complex. The interaction between VAMP3 and the gM/gN complex was also confirmed in HHV-6A-infected cells. VAMP3 and gM/gN proteins colocalized at the TGN in cells coexpressing gM and gN, and in HHV-6A-infected cells. This interaction was observed only when gM/gN formed a complex, indicating that the interaction is required for gM/gN complex formation. Previously, we reported that the localization of HHV-6A gM to the TGN was necessary for its interaction with gN (Kawabata *et al.*, 2012). Therefore, the interaction between the gM/gN complex and VAMP3 might also occur at the TGN. It is still not known whether the interaction between VAMP3 and gM requires gM/gN complex formation. Transport of gM to the TGN might be required for this interaction.

VAMP3 also colocalized with CD63, which is a marker of late endosome in HHV-6A-infected cells. In cells transiently expressing gM and gN, however, VAMP3 colocalized with TGN46, but not CD63. This suggests that in infected cells, the localization of VAMP3 may be modified through its interaction with gM/gN, thereby possibly allowing it to localize to the other organelles, such as the late endosome.

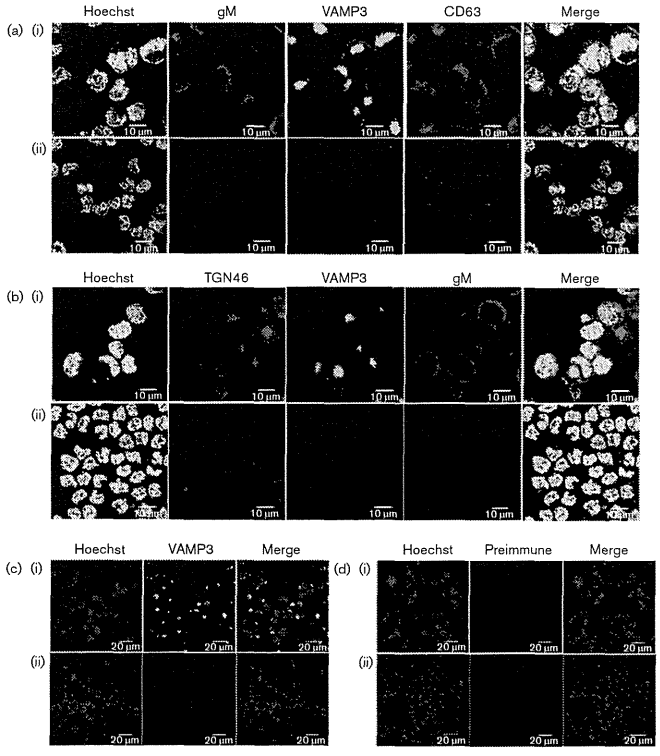

Fig. 3. Colocalization of gM, VAMP3 and CD63, or gM, VAMP3 and TGN46 in HHV-6A-infected cells. HHV-6A-infected [a(i), b(i)] or mock-infected [a(ii), b(ii)] HSB-2 cells were harvested at 96 h post-infection and fixed. The cells were stained with antibodies against VAMP3, gM and CD63 as well as with Hoechst 33258 (a), or VAMP3, gM and TGN46 as well as with Hoechst 33258 (b). Costained areas appear white in the merged panel. Bars, 10 μm. HHV-6A-infected [c(i), d(i)] or mock-infected [c(ii), d(ii)] cells were stained with guinea pig antisera against VAMP3 (c) or preimmune sera obtained from the same guinea pig as well as with Hoechst 33258 (d). Bars, 20 μm.

We also found that VAMP3 was incorporated into virions. As the gM/gN complex is expressed on virions and exosomes, complex-associated VAMP3 would be transported along with the gM/gN complex and then released via the exosomal release pathway (Mori *et al.*, 2008).

Although the function of VAMP3 in HHV-6A-infected cells is not known, its interaction with the gM/gN complex may modify the cellular machinery in infected cells. As VAMP3 is incorporated into virions and exosomes, its primary function (to facilitate membrane fusion) may be lost in infected cells. Overexpression of VAMP3 did not affect HHV-6 growth (data not shown). Several v-SNARE proteins with functions similar to those of VAMP3 have been identified (Borisovska *et al.*, 2005). Therefore, the function of VAMP3 may be redundant in HHV-6A-infected cells. It is still not known whether v-SNAREs, including VAMP3, are required for HHV-6 infection. Further studies will be required to address these questions.

METHODS

Cells and viruses. The HSB-2 T-cell line was cultured in RPMI 1640 medium (Nissui) supplemented with 8% FBS. Human embryonic

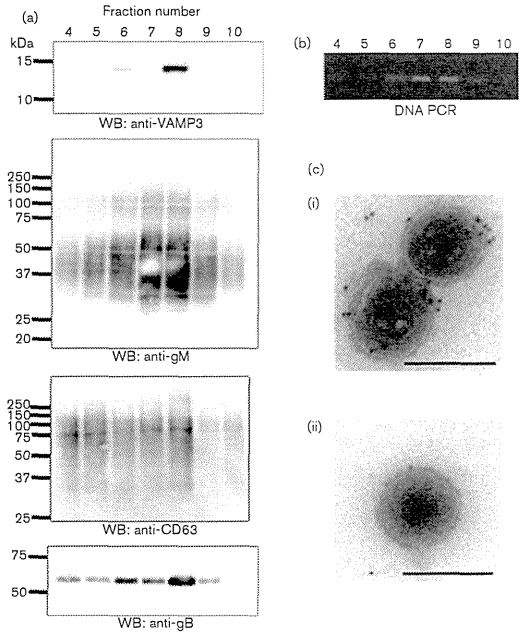

Fig. 4. The presence of VAMP3 in HHV-6A virions and exosomes. Exosome fractions containing virions were purified from the culture medium of HHV-6A-infected cells by sucrose density-gradient centrifugation and then analysed by Western blotting (a), DNA PCR (b) and electron microscopy (c). (a) Western blot analysis of the sucrose density-gradient fractions with anti-VAMP3, anti-gM, anti-CD63 or anti-gB Abs. (b) Viral DNA was detected in the fractions by PCR with HHV-6A specific primers. The numbers above the PCR image showed the fraction numbers. (c) Immunogold localization of VAMP3 on the HHV-6A virions. Purified virions (fraction 8) were labelled with antisera against VAMP3 (i) or without primary antibody (ii). Bars, 200 nm.

kidney cells (293T cells) and HeLa cells were cultured in Dulbecco's modified Eagle's medium supplemented with 8% FBS. The HHV-6A strain GS was propagated and titrated in HSB-2 cells. HHV-6A cell-free virus was prepared as previously described (Akkapaiboon *et al.*, 2004). Cord blood mononuclear cells (CBMC) were used for virus propagation (Mori *et al.*, 2004). CBMCs were kindly provided by K. Adachi (Minoh Hospital, Minoh, Japan) and H. Yamada (Kobe University Graduate School of Medicine, Kobe, Japan) and purchased from the RIKEN Cell Bank (BioResource Center). For the usage of CBMCs, the study was approved by the ethics committee of each institution.

Antibodies. Rabbit antibody (Ab) specific for HHV-6A gM or gB (Mori *et al.*, 2008), an AgM-1 mAb against gM (Kawabata *et al.*, 2012), and a U14 mAb against HHV-6 U14 (Takemoto *et al.*, 2005) were used. mAbs against CD63 (clone CLB-gran/12, 435; Sanquin) and α-tubulin (clone B-5-1-2; Sigma), a sheep polyclonal Ab against TGN46 (AbD Serotec), a rabbit polyclonal Ab against VAMP3 (BioReagents) and a goat polyclonal Ab against VAMP3 (Santa Cruz) were used. Anti-HA (clone HA-7; Sigma) and anti-FLAG (clone M2; Sigma) antibodies were also used. Alexa Fluor 594-conjugated donkey anti-sheep IgG (Molecular Probes), Alexa Fluor 594-conjugated donkey anti-rabbit IgG (Molecular Probes), FITC-conjugated affinity pure $F(ab')_2$ fragment goat anti-guinea pig IgG (Jackson ImmunoResearch Laboratories), and Cy5-conjugated donkey anti-mouse IgG (Jackson ImmunoResearch Laboratories) were used as secondary antibodies. An anti-VAMP3 monospecific Ab was produced by subjecting guinea pigs to three rounds of immunization with the antigen, which was then expressed in *Escherichia coli* and purified (Mori *et al.*, 2008).

Immunofluorescence assay. The IFA was performed as described previously (Akkapaiboon *et al.*, 2004; Mori *et al.*, 2004). Specific immunofluorescence was observed under a confocal laser-scanning microscope (FluoView FV1000; Olympus).

Plasmid construction. The HA-tagged gM- and FLAG-tagged gN-expressing plasmids were described previously (Kawabata *et al.*, 2012). The pCAGGS plasmid was kindly provided by Jun-ichi Miyazaki (Osaka University, Japan) (Niwa *et al.*, 1991). To express the recombinant protein, the following primer pair was used to amplify inserts from HSB-2 cells cDNA: for named GST-VAMP3, VAMP3FbamHI (5′-ACCGGATCCTCTACAGGTCCAACTGCTGC-CACT-3′) and VAMP3rsall (5′-ACCGTCGACTTACTTGCAATTCT-TCCACCAATATTTC-3′). The PCR products were inserted into the pGEX-4T1 vector (GE Healthcare).

Plasmid transfection. HeLa cells were transfected with the expression plasmids using Lipofectamine 2000 (Invitrogen) according to the manufacturer's instructions. The 293T cells were transfected using the calcium phosphate method as described previously (Koshizuka *et al.*, 2010).

Identification of gM/gN-interacting proteins. Plasmids expressing HA-tagged gM and FLAG-tagged gN were cotransfected into 293T cells. Cotransfection of gM and pCAGGS into 293T cells was performed as a control. At 72 h post-transfection, the cells were lysed in TNE buffer (0.01 M Tris/HCl, pH 7.4, 0.15 M NaCl, 1 mM EDTA, 1% Nonidet-P-40). After centrifugation at 200 000 *g* for 1 h, the

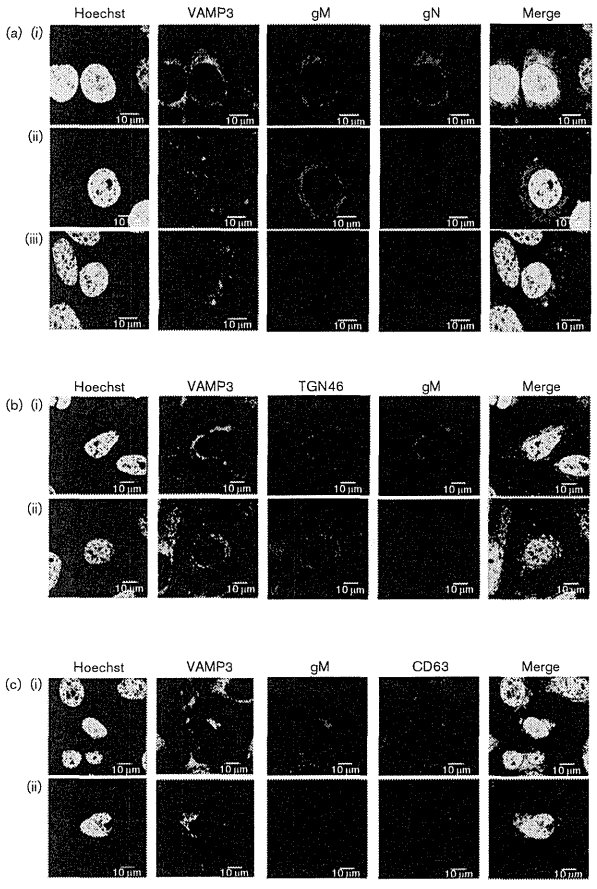

Fig. 5. Subcellular localization of VAMP3 with the gM/gN complex in HeLa cells transiently expressing gM and gN. HeLa cells were transfected with plasmids expressing gM and gN [a(i), b(i), c(i)], gM and the empty vector [a(ii)], or without vectors [a(iii), b(ii), c(ii)]. The cells were harvested at 48 h post-transfection and fixed. (a) The cells were stained with antibodies against gM, FLAG (for gN) and VAMP3 as well as with Hoechst 33258. (b) Cells were stained with antibodies against gM, TGN46 and VAMP3 as well as Hoechst 33258. (c) Cells were stained with antibodies against gM, CD63 and VAMP3 as well as with Hoechst 33258. Co-stained areas appear white or yellow in the merged panel. Bars, 10 μm.

supernatants were incubated overnight at 4 °C with an anti-HA antibody conjugated to protein G Sepharose (GE Healthcare). The protein-anti-HA conjugated beads were then washed with lysis buffer and the bound proteins were eluted with 0.1 M glycine/HCl (pH 2.8). After the beads were removed by centrifugation, the supernatants were neutralized by adding 1 M Tris-HCl (pH 9.5). The eluted proteins were then solubilized with sample buffer, separated on a NuPAGE SDS-PAGE system (Invitrogen), and examined by silver staining. Specific bands were analysed by LC-MS/MS to identify the coimmunoprecipitated proteins (Shevchenko *et al.*, 1996; Tang *et al.*, 2013).

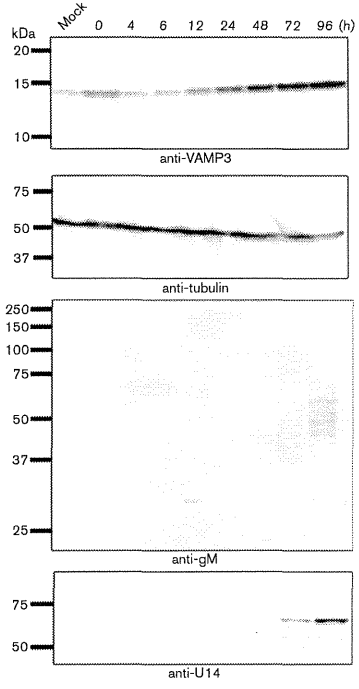

Fig. 6. *Kinetics of VAMP3 protein expression in HHV-6A-infected cells.* Whole-cell lysates collected at the indicated time points (h) were analysed by Western blotting. The numbers beside the panels indicate the molecular masses (kDa).

Western blotting. Western blotting was performed as described previously (Akkapaiboon *et al.*, 2004).

Isolation of virion fractions. Virions containing exosomes were collected from the cell culture medium by differential centrifugation and fractionated with a linear sucrose gradient, as described previously (Mori *et al.*, 2008). The fractions were analysed by Western blotting, DNA PCR, and electron microscopy.

Electron microscopy. Immunogold labelling of virions was performed as described previously (Mori *et al.*, 2008). The samples were examined under a Hitachi H-7650 electron microscope.

ACKNOWLEDGEMENTS

We thank E. Moriishi (National Institute of Biomedical Innovation), Mayuko Hayashi and Megumi Ota (Kobe University) for technical assistance, J. Miyazaki (Osaka University) for providing reagents, and K. Adachi (Minoh City Hospital) and H. Yamada (Kobe University) for the CBMCs. This work was supported by a Grant-in-Aid for Scientific Research (B) from the Japan Society for the Promotion of Science (JSPS).

REFERENCES

Ablashi, D. V., Balachandran, N., Josephs, S. F., Hung, C. L., Krueger, G. R., Kramarsky, B., Salahuddin, S. Z. & Gallo, R. C. (1991). Genomic polymorphism, growth properties, and immunologic variations in human herpesvirus-6 isolates. *Virology* **184**, 545–552.

Ablashi, D., Agut, H., Alvarez-Lafuente, R., Clark, D. A., Dewhurst, S., Diluca, D., Flamand, L., Frenkel, N., Gallo, R. & other authors (2014). Classification of HHV-6A and HHV-6B as distinct viruses. *Arch Virol* **159**, 863–870.

Akkapaiboon, P., Mori, Y., Sadaoka, T., Yonemoto, S. & Yamanishi, K. (2004). Intracellular processing of human herpesvirus 6 glycoproteins Q1 and Q2 into tetrameric complexes expressed on the viral envelope. *J Virol* **78**, 7969–7983.

Aubin, J. T., Collandre, H., Candotti, D., Ingrand, D., Rouzioux, C., Burgard, M., Richard, S., Huraux, J. M. & Agut, H. (1991). Several groups among human herpesvirus 6 strains can be distinguished by Southern blotting and polymerase chain reaction. *J Clin Microbiol* **29**, 367–372.

Baines, J. D. & Roizman, B. (1991). The open reading frames UL3, UL4, UL10, and UL16 are dispensable for the replication of herpes simplex virus 1 in cell culture. *J Virol* **65**, 938–944.

Borisovska, M., Zhao, Y., Tsytsyura, Y., Glyvuk, N., Takamori, S., Matti, U., Rettig, J., Südhof, T. & Bruns, D. (2005). v-SNAREs control exocytosis of vesicles from priming to fusion. *EMBO J* **24**, 2114–2126.

Campadelli-Fiume, G., Guerrini, S., Xiaoming, L. & Foà-Tomasi, L. (1993). Monoclonal antibodies to glycoprotein B differentiate human herpesvirus 6 into two clusters, variants A and B. *J Gen Virol* **74**, 2257–2262.

Chandran, B., Tirawatnapong, S., Pfeiffer, B. & Ablashi, D. V. (1992). Antigenic relationships among human herpesvirus-6 isolates. *J Med Virol* **37**, 247–254.

Dijkstra, J. M., Visser, N., Mettenleiter, T. C. & Klupp, B. G. (1996). Identification and characterization of pseudorabies virus glycoprotein gM as a nonessential virion component. *J Virol* **70**, 5684–5688.

Galli, T., Chilcote, T., Mundigl, O., Binz, T., Niemann, H. & De Camilli, P. (1994). Tetanus toxin-mediated cleavage of cellubrevin impairs exocytosis of transferrin receptor-containing vesicles in CHO cells. *J Cell Biol* **125**, 1015–1024.

Hobom, U., Brune, W., Messerle, M., Hahn, G. & Koszinowski, U. H. (2000). Fast screening procedures for random transposon libraries of cloned herpesvirus genomes: mutational analysis of human cytomegalovirus envelope glycoprotein genes. *J Virol* **74**, 7720–7729.

Hu, C., Hardee, D. & Minnear, F. (2007). Membrane fusion by VAMP3 and plasma membrane t-SNAREs. *Exp Cell Res* **313**, 3198–3209.

Jahn, R. & Scheller, R. H. (2006). SNAREs–engines for membrane fusion. *Nat Rev Mol Cell Biol* **7**, 631–643.

Jahn, R., Lang, T. & Südhof, T. C. (2003). Membrane fusion. *Cell* **112**, 519–533.

Kawabata, A., Jasirwan, C., Yamanishi, K. & Mori, Y. (2012). Human herpesvirus 6 glycoprotein M is essential for virus growth and requires glycoprotein N for its maturation. *Virology* **429**, 21–28.

Koshizuka, T., Ota, M., Yamanishi, K. & Mori, Y. (2010). Characterization of varicella-zoster virus-encoded ORF0 gene–comparison of parental and vaccine strains. *Virology* **405**, 280–288.

Krzyzaniak, M. A., Mach, M. & Britt, W. J. (2009). HCMV-encoded glycoprotein M (UL100) interacts with Rab11 effector protein FIP4. *Traffic* **10**, 1439–1457.

Lawrence, G. L., Nicholas, J. & Barrell, B. G. (1995). Human herpesvirus 6 (strain U1102) encodes homologues of the conserved herpesvirus glycoprotein gM and the alphaherpesvirus origin-binding protein. *J Gen Virol* **76**, 147–152.

Luftman, K., Hasan, N., Day, P., Hardee, D. & Hu, C. (2009). Silencing of VAMP3 inhibits cell migration and integrin-mediated adhesion. *Biochem Biophys Res Commun* **380**, 65–70.

McMahon, H. T., Ushkaryov, Y. A., Edelmann, L., Link, E., Binz, T., Niemann, H., Jahn, R. & Südhof, T. C. (1993). Cellubrevin is a ubiquitous tetanus-toxin substrate homologous to a putative synaptic vesicle fusion protein. *Nature* **364**, 346–349.

Mohrmann, R. & Sørensen, J. B. (2012). SNARE requirements en route to exocytosis: from many to few. *J Mol Neurosci* **48**, 387–394.

Mori, Y. (2009). Recent topics related to human herpesvirus 6 cell tropism. *Cell Microbiol* **11**, 1001–1006.

Mori, Y., Akkapaiboon, P., Yonemoto, S., Koike, M., Takemoto, M., Sadaoka, T., Sasamoto, Y., Konishi, S., Uchiyama, Y. & Yamanishi, K. (2004). Discovery of a second form of tripartite complex containing gH-gL of human herpesvirus 6 and observations on CD46. *J Virol* **78**, 4609–4616.

Mori, Y., Koike, M., Moriishi, E., Kawabata, A., Tang, H., Oyaizu, H., Uchiyama, Y. & Yamanishi, K. (2008). Human herpesvirus-6 induces MVB formation, and virus egress occurs by an exosomal release pathway. *Traffic* **9**, 1728–1742.

Niwa, H., Yamamura, K. & Miyazaki, J. (1991). Efficient selection for high-expression transfectants with a novel eukaryotic vector. *Gene* **108**, 193–199.

Osterrieder, N., Neubauer, A., Brandmuller, C., Braun, B., Kaaden, O. R. & Baines, J. D. (1996). The equine herpesvirus 1 glycoprotein gp21/22a, the herpes simplex virus type 1 gM homolog, is involved in virus penetration and cell-to-cell spread of virions. *J Virol* **70**, 4110–4115.

Polgár, J., Chung, S. H. & Reed, G. L. (2002). Vesicle-associated membrane protein 3 (VAMP-3) and VAMP-8 are present in human platelets and are required for granule secretion. *Blood* **100**, 1081–1083.

Roizmann, B., Desrosiers, R. C., Fleckenstein, B., Lopez, C., Minson, A. C., Studdert, M. J. & The Herpesvirus Study Group of the International Committee on Taxonomy of Viruses (1992). The family *Herpesviridae*: an update. *Arch Virol* **123**, 425–449.

Rothman, J. E. (1994). Mechanisms of intracellular protein transport. *Nature* **372**, 55–63.

Shevchenko, A., Wilm, M., Vorm, O. & Mann, M. (1996). Mass spectrometric sequencing of proteins silver-stained polyacrylamide gels. *Anal Chem* **68**, 850–858.

Söllner, T., Whiteheart, S. W., Brunner, M., Erdjument-Bromage, H., Geromanos, S., Tempst, P. & Rothman, J. E. (1993). SNAP receptors implicated in vesicle targeting and fusion. *Nature* **362**, 318–324.

Takemoto, M., Koike, M., Mori, Y., Yonemoto, S., Sasamoto, Y., Kondo, K., Uchiyama, Y. & Yamanishi, K. (2005). Human herpesvirus 6 open reading frame U14 protein and cellular p53 interact with each other and are contained in the virion. *J Virol* **79**, 13037–13046.

Tang, H., Serada, S., Kawabata, A., Ota, M., Hayashi, E., Naka, T., Yamanishi, K. & Mori, Y. (2013). CD134 is a cellular receptor specific for human herpesvirus-6B entry. *Proc Natl Acad Sci U S A* **110**, 9096–9099.

Tayeb, M. A., Skalski, M., Cha, M. C., Kean, M. J., Scaife, M. & Coppolino, M. G. (2005). Inhibition of SNARE-mediated membrane traffic impairs cell migration. *Exp Cell Res* **305**, 63–73.

Tischer, B. K., Schumacher, D., Messerle, M., Wagner, M. & Osterrieder, N. (2002). The products of the UL10 (gM) and the UL49.5 genes of Marek's disease virus serotype 1 are essential for virus growth in cultured cells. *J Gen Virol* **83**, 997–1003.

Veale, K. J., Offenhäuser, C., Lei, N., Stanley, A. C., Stow, J. L. & Murray, R. Z. (2011). VAMP3 regulates podosome organisation in macrophages and together with Stx4/SNAP23 mediates adhesion, cell spreading and persistent migration. *Exp Cell Res* **317**, 1817–1829.

Yamagishi, Y., Sadaoka, T., Yoshii, H., Somboonthum, P., Imazawa, T., Nagaike, K., Ozono, K., Yamanishi, K. & Mori, Y. (2008). Varicella-zoster virus glycoprotein M homolog is glycosylated, is expressed on the viral envelope, and functions in virus cell-to-cell spread. *J Virol* **82**, 795–804.

Yamanishi, K., Shiraki, K., Kondo, T., Okuno, T., Takahashi, M., Asano, Y. & Kurata, T. (1988). Identification of human herpesvirus-6 as a causal agent for exanthem subitum. *Lancet* **331**, 1065–1067.

Journal of proteome research

Article

pubs.acs.org/jpr

Identification of Sialylated Glycoproteins in Doxorubicin-Treated Hepatoma Cells with Glycoproteomic Analyses

Kanako Azuma,[†] Satoshi Serada,[‡] Shinji Takamatsu,[†] Naoko Terao,[†] Shunsaku Takeishi,[§] Yoshihiro Kamada,[†] Tetsuji Naka,[‡] and Eiji Miyoshi*[,†]

[†]Department of Molecular Biochemistry & Clinical Investigation, Osaka University Graduate School of Medicine, Osaka 565-0871, Japan

[‡]Laboratory for Immune Signal, National Institute of Biomedical Innovation, Osaka 567-0085, Japan

[§]Department of Gastroenterology and Oncology, Institute of Health Biosciences, The University of Tokushima Graduate School, Tokushima 770-0855, Japan

Supporting Information

ABSTRACT: Sialylation is one of the most important types of glycosylation involved in carcinogenesis and establishment of cancer stemness. We previously showed that increased sialylation is a characteristic glycan change in cancer stem cells (CSCs) from hepatocellular carcinoma. However, the identities of glycoproteins targeted for sialylation remain unknown. In the present study, we identified glycoproteins targeted for sialylation in doxorubicin (DXR)-treated hepatocarcinoma cell line, Huh7, using glycoproteomic analyses. Since CSCs constitute a small subset of cells within carcinoma cell lines, it is difficult to identify sialylated proteins using general glycoproteomic strategies. It is known that treatment with anticancer drug can condense CSCs, we used DXR to concentrate CSCs. In DXR-treated Huh7 cells, isobaric tag for relative and absolute quantitation (iTRAQ) analysis identified 17 sialylated glycoproteins. Most of the identified glycoproteins were cancer-associated proteins. Furthermore, two proteins of approximately 70 kDa were detected using *Sambucus sieboldoana* agglutinin (SSA) blot analysis and identified as beta-galactosidase and alpha-2-HS-glycoprotein (fetuin-A) by SSA precipitation followed by liquid chromatography-tandem mass spectrometry analyses. Sialylation levels of fetuin-A were increased in DXR-treated Huh7 cell lysates. These changes in sialylation of glycoproteins might be involved in the establishment of cancer stemness.

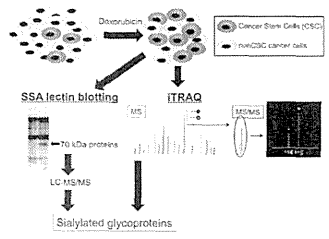

KEYWORDS: *sialylation, cancer stem cells, doxorubicin, hepatoma, glycoproteomics*

INTRODUCTION

A growing body of evidence suggests that tumors are frequently composed of heterogeneous cell types and that tumor initiation and growth are driven by a small subset of cells, termed cancer stem cells (CSCs), or tumor-initiating cells.[1−3] Several lines of research have indicated that CSCs can be preferentially resistant to many current therapies, including various chemotherapeutic agents and radiation treatment.[4−7] Thus, therapeutic strategies that effectively target CSCs could have a major impact on cancer patient survival. There are many reports on CSC markers, which include CD13,[8] CD44,[9,10] epithelial cell adhesion molecule (EpCAM),[11] and CD133.[9,12,13] These CSC markers have been used for identifying or concentrating CSCs in each type of cancer. It is unknown whether pure CSCs or whether heterogeneous populations containing CSC-like cells, should be targets for therapeutic strategies. Glycans are often attached to proteins and lipids on the cell surface and structurally and functionally modify these molecules. Glycans consist of several kinds of monosaccharides and show great structural diversity. Research in the field of glycobiology has revealed diverse and complex biological roles for these glycans.[14] The structures and amounts of glycans present on the cell surface change dramatically during development and differentiation.[15] We have recently reported that sialylated glycans are useful markers for CSC-like cells in hepatoma cell lines.[16] Glycomic analysis using a lectin microarray showed marked binding of *Sambucus sieboldoana* agglutinin (SSA) to a $CD133^{+}CD13^{+}$ cell subpopulation within hepatoma cell lines. SSA lectin recognizes α2, 6-sialic acid.[16] Sialic acid is one of the building blocks of glycans and is generally found at the outermost ends of the glycan chains of glycoproteins and glycolipids. Thus, sialic acid is associated with many physiological and pathological events, including binding to infectious pathogens, regulation of immune responses, and tumor malignancy.[17] In particular, the alteration of sialic acid moieties is associated with cancer cell behavior, such as invasiveness and metastasis.[18−23] Glycan changes are involved in development and differentiation, and sialic acid is one of the most important glycosylations involved in these processes.[24]

Special Issue: Proteomics of Human Diseases: Pathogenesis, Diagnosis, Prognosis, and Treatment

Received: May 1, 2014
Published: August 26, 2014

In terms of glycoproteomic analyses, the identification of target proteins for each characteristic oligosaccharide structure is very important.[25] However, using the conventional strategy, which involves pooling and concentrating the CSC fraction using CD markers and lectins, it was not easy to obtain appropriate amounts of proteins for glycomic analyses. In general, CSC or CSC-like cells are resistant to anticancer drug treatment. For example, a CD133 and SSA double-positive population was resistant to several kinds of anticancer drug treatments such as 5-fluorouracil (5-FU) (Supplementary Figure 1). Hermann et al. also showed that the number of CD133-positive cells increased in human pancreatic cancer cells treated with gemcitabine.[26] These results suggest that short-term treatment with anticancer drugs can be used to easily concentrate CSCs. Among emerging proteomic technologies, isobaric tags for relative and absolute quantitation (*i*TRAQ) is a shotgun-based technique, which allows the concurrent identification and relative quantification of hundreds of proteins from different biological samples in a single experiment.[27,28] Whereas iTRAQ analysis leads to a more comprehensive analysis of sialylated proteins, the SSA lectin precipitation technique followed by liquid chromatography–tandem mass spectrometry (LC–MS/MS) analysis allows for protein enrichment, which aids in the identification of specific target proteins.

In the present study, we investigated characteristic glycan structures in the doxorubicin (DXR)-treated human hepatoma cell line Huh7, and further identified their target glycoproteins using iTRAQ and SSA lectin precipitation followed by LC–MS/MS. In addition, the expression levels of these proteins were confirmed using Western blotting, and their biological significance in CSC functions is discussed.

MATERIALS AND METHODS

Cell Culture and Cell Treatments

The human hepatoma cell line Huh7 was obtained from American Type Culture Collection (ATCC, Manassas, VA, USA) and cultured in RPMI 1640 (Sigma, St. Louis, MO, USA) medium containing 10% fetal bovine serum (Invitrogen, Carlsbad, CA, USA), supplemented with 100 units/mL penicillin G and 100 μg/mL streptomycin in a 37 °C incubator under a humidified atmosphere containing 5% CO_2. The cells were seeded into 100 mm dishes at 1×10^6 cells/dish. After 6 h, doxorubicin (DXR) (Sigma) was added to the culture medium (5 μg/mL). The cells were harvested after 48 h of exposure to DXR, and the culture media were harvested as conditioned media for the following analyses.

Lectin Microarray

Patterns of oligosaccharide structures in Huh7 cells treated with or without DXR were investigated by means of evanescent-field fluorescence-assisted lectin microarray. Forty-five types of lectins were immobilized on a glass slide in triplicate. The procedure has been described in detail, previously.[29] Briefly, total cellular proteins in phosphate buffered saline (PBS) containing 1% Triton X-100 were labeled with Cy3-succinimidyl ester (GE Healthcare, Chalfont St. Giles, U.K.) at room temperature (RT) for 1 h in the dark. Excess reagent was removed by gel filtration chromatography. The resultant Cy3-labeled protein solution was applied to a lectin microarray. After incubation at 20 °C for 15 h, the glass slide was scanned with an evanescent-field fluorescence scanner, GlycoStation (GP Biosciences Ltd., Kanagawa, Japan). All of the data were analyzed using Array Pro Analyzer version 4.5 (Media Cybernetics, Inc., Bethesda, MD, USA). The net intensity value for each spot was calculated by subtracting the background value. The signal intensity value for each lectin was expressed as the average of the net intensity values for three spots. The signal from wheat germ agglutinin (WGA) was used to normalize the signal intensity of each lectin because binding to WGA lectin was relatively stable and similar using different cell types.

Mass Spectrometric Analysis

NanoLC–MS/MS analyses were performed on LTQ-Orbitrap XL (Thermo Fisher Scientific, Waltham, MA) equipped with nano-ESI source and coupled to Paradigm MG4 pump (Michrom Bioresources, Auburn, CA) and autosampler (HTC PAL, CTC Analytics, Zwingen, Switzerland). Peptide mixtures were separated on MagicC18AQ column (100 mm × 150 mm, 3.0 μm particle size, 300 Å, Michrom Bioresources) with a flow rate of 500 nL/min. A linear gradient of 5–30% B in 80 min, 30–95% B in 10 min, and 95% B for 4 min and finally decreased to 5% B was employed (A = 0.1% formic acid in 2% acetonitrile; B = 0.1% formic acid in 90% acetonitrile). Intact peptides were detected in the Orbitrap at 30,000 resolution. Up to three CID and HCD spectra were acquired in a data-dependent acquisition mode following each full scan (m/z, 400–1500). The mass spectrometer was operated in positive ion mode.

Preparation of Labeled Peptides for Isobaric Tags for Relative and Absolute Quantitation (iTRAQ) Analysis

Each protein sample (adjusted to 4.1 mg) was digested with 50 μg of Trypsin-TPCK Solution (Applied Biosystems, Framingham, MA, USA) at 37 °C overnight and sialylated proteins were isolated using *Sambucus sieboldiana* agglutinin (SSA) covalently linked to agarose beads (SSA-agarose) (J-Oil Mills, Inc., Tokyo, Japan). After applying to an SSA-agarose column, each sample was incubated for 6 h at 4 °C. The SSA-Agarose column was washed with 1 mL of 50 mM Tris HCl [pH 7.4] buffer five times. Bound peptides were eluted from the SSA-Agarose column using 1 mL of the elution buffer (0.2 *M* lactose) three times. The eluted samples were deglycosylated with glycopeptidase F. Deglycosylated peptides were desalted and labeled with iTRAQ reagents (Applied Biosystems) according to the manufacturer's instructions. Proteins from Huh7 cells, treated with or without DXR and eluted from SSA agarose, were labeled with iTRAQ reagents 114 and 115, respectively. All labeled peptide samples were mixed and fractionated as described previously.[30]

iTRAQ Data Analysis

Protein identification and quantification for iTRAQ analysis was carried out using Proteome Discoverer v.1.3 (Thermo Fisher Scientific) using the MASCOT algorithm against Swiss-Prot protein database (Swiss-Prot_2012_06 536,489 entries). Taxonomy was set to *Homo sapiens* (20,312 entries). Search parameters for peptide and MS/MS mass tolerance were 10 ppm and 0.8 Da, respectively, with allowance for two missed cleavages made from the trypsin digest. Carbamidomethylation (Cys) and iTRAQ4plex (Lys, N-terminal) were specified as static modifications, whereas deamidation (Asn, Gln), iTRAQ4plex (Tyr), and oxidation (Met) were specified as dynamic modifications in the database search. When deamidation of Asn were detected, the amino acids were considered as glycan binding site because glycopeptidase F treatment convert glycosylated Asn residue to Asp. Mascot results were filtered with the integrated Percolator based filter using a false discovery rate <1% (based on PSMs). Relative protein abundances were calculated using the ratio of iTRAQ reporter ion in the MS/MS scan. List of the glycoproteins identified in iTRAQ analysis was represented in Supplementary Table 1.

Protein Identification by Mass Spectrometry

The gels were stained with the Silver Stain MS kit according to the manufacturer's instruction (WAKO Pure Chemical Industries, Ltd., Osaka, Japan). Protein spots in a silver-stained gel, corresponding to positive spots on Western blot membranes, were excised from the gel and digested in gel according to a previously described method,[31,32] using sequencing grade modified trypsin (Promega, Inc., Madison, WI). Digested peptides were then extracted with 5% TFA in acetonitrile (acetonitrile/DW 50:45), sonicated for 5 min and concentrated by evaporation. Dried peptides were dissolved in 0.1% TFA (v/v) and 2% acetonitrile (v/v) for subsequent LC–MS/MS analysis. NanoLC–MS/MS analyses were performed on a LTQ-Orbitrap XL mass spectrometer (Thermo Fisher Scientific) equipped with a nano-ESI source (AMR) and coupled to a Paradigm MG4 pump (Michrom Bioresources) and an autosampler (HTC PAL, CTC Analytics). A spray voltage of 1800 V was applied. The peptide mixture was separated on a Magic C18AQ column (100 μm × 150 mm, 3.0 μm particle size, 300 Å, Michrom Bioresources) with a flow rate of 500 nL/min. The linear gradient of 5% to 45% B in 30 min, 45% to 95% B in 0.1 min, and 95% B for 2 min and finally decreased to 5% B was employed (A = 0.1% formic acid in 2% acetonitrile; B = 0.1% formic acid in 90% acetonitrile). Intact peptides were detected in the Orbitrap at 60,000 resolutions. For LC–MS/MS analysis, 6 precursor ions were selected for subsequent MS/MS scans in a data-dependent acquisition mode following each full scan (m/z, 350–1500). A lock mass function was used for the LTQ-Orbitrap to obtain constant mass accuracy during gradient analysis. Peptides and proteins were identified by means of automated database search using Proteome Discoverer v.1.3 (Thermo Fisher Scientific) against human of Swiss-Prot protein database (Swiss-Prot_2012_06) with a precursor mass tolerance of 10 ppm, a fragment ion mass tolerance of 0.8 Da, and strict trypsin specificity, allowing for up to two missed cleavages. Carbamidomethylation of cysteine was set as a fixed modification, and oxidation of methionines was allowed as dynamic modifications. Raw data of MS/MS analysis was represented in Supplementary Figure 2.

Lectin Blot Analysis

Huh7 cells were quickly harvested from a 100 mm dish in ice-cold PBS. After precipitation by centrifugation at 2000 rpm for 5 min at 4 °C, the cells were resuspended in TNE buffer (10 mM Tris-HCl [pH 7.8], 1% NP40, 1 mM EDTA, and 0.15 *M* NaCl) containing a protease inhibitor cocktail (Roche, Mannheim, Germany) and then placed on ice for 30 min to allow solubilization. Samples were then centrifuged at 15,000 rpm for 15 min at 4 °C, and the supernatants were collected as cell lysates. Samples were quantitated using a bicinchoninic acid (BCA) assay kit (Pierce, Rockford, IL, USA).

In each experiment, duplicate samples were subjected to 8% sodium dodecyl sulfate polyacrylamide gel electrophoresis (SDS-PAGE) under reducing conditions. One gel was subjected to Coomassie Brilliant Blue (CBB) R-250 staining and another was transferred to a polyvinyl difluoride (PVDF) membrane (Millipore Corp., Billerica, MA, USA) for lectin blot analysis, using SSA, *Leukoagglutinating phytohemagglutinin* (L4-PHA), *Aleuria aurantia* lectin (AAL), and *Datura stramonium* (DSA). After blocking with PBS containing 3% bovine serum albumin (BSA) overnight at 4 °C, each membrane was incubated in 1:2500–1:10000 diluted biotinylated SSA, L4-PHA, AAL, and DSA (J-Oil Mills, Inc., Tokyo, Japan) for 20 min at RT. The membranes were then washed three times with Tris-buffered saline containing 0.05% Tween-20 (TBST) (pH 7.4) and incubated with 1:2500 diluted avidin–peroxidase conjugates (ABC kits, Vector Res. Corp., Burlingame, CA, USA) for 20 min at RT. The membrane was again washed three times with TBST and then developed using an enhanced chemiluminescence system, Immobilon Western (Millipore), according to the manufacturer's protocol.

Immunoblot Analysis

Cell lysates and conditioned media were subjected to 8% SDS-PAGE under reducing conditions and then transferred to a PVDF membrane (Millipore). After blocking with PBS containing 5% skim milk for 1 h at RT, each membrane was incubated overnight at 4 °C with the following primary antibodies diluted 1:1000–1:5000: anti-HYOU1 (Abnova, Taipei, Taiwan), anti-P4HA1 (Abnova, Taipei City, Taiwan), anti-LAMP1 (Abcam Inc., Cambridge, MA, USA), anti-LAMP2 (Santa Cruz Biotechnology Inc., Santa Cruz, CA, USA), antibeta-galactosidase (Santa Cruz Biotechnology), antifetuin-A (Santa Cruz Biotechnology), or anti-β-actin (Cell Signaling, Beverly, MA, USA) for 60 min at RT. The dilution ratios for these antibodies ranged from 1:1000 to 1:5000. The membranes were then washed three times with Tris-buffered saline containing 0.05% Tween-20 (TBST) (pH 7.4) and incubated with 1:5000 diluted horseradish peroxidase conjugated with the appropriate secondary antibody for 30 min at RT. The membranes were again washed three times and developed using an Immobilon Western (Millipore).

Lectin Precipitation

Extracted protein (100 μg) was incubated with 40 μL of SSA-agarose overnight with shaking at 4 °C. Precipitated proteins were washed in 50 mM Tris HCl [pH 7.4] and then boiled in SDS sample buffer. Ten microliters of precipitated proteins were subjected to 8% SDS-PAGE. The gel was stained with Silver Stain MS Kits (Wako, Osaka, Japan). Protein bands were excised from the gel and digested with sequencing grade trypsin (Promega) as described previously.[33]

Neuraminidase/*N*-Glycanase Treatments

The extracted proteins (100 μg) were incubated overnight at 37 °C with 200 mU/mL of neuraminidase (Roche, Nutley, NJ, USA) in 50 mM AcOH buffer [pH 5.5] containing 4 mM $CaCl_2$ and 100 μg/mL BSA. In addition, 100 μg of the extracted proteins were incubated with glycopeptidase F (Takara Bio Inc., Otsu, Japan) according to the manufacturer's protocol. The cell lysates were subsequently boiled in SDS-PAGE sample buffer, electrophoresed on 8% SDS PAGE, and then transferred onto a PVDF membrane (Millipore). After blocking with TBST containing 5% skim milk at 4 °C overnight, Western blot analysis for fetuin-A was performed using antifetuin-A antibody.[34] Briefly, 1:5000 diluted antifetuin-A was incubated in TBST buffer containing 5% skim milk for 1 h at RT. After washing the membrane three times with TBST, it was incubated for 1 h at RT with the secondary antibody, horseradish peroxidase-conjugated antirabbit-IgG (Promega), diluted 1:5000. It was again washed three times and developed with an Immobilon Western (Millipore).

Immunofluorescence Confocal Microscopy

Huh7 cells were seeded in 35 mm dishes at 3×10^5 cells/dish. After 6 h, DXR was added to the culture medium (5 μg/mL). After 48 h of exposure to DXR, cells were washed once in PBS

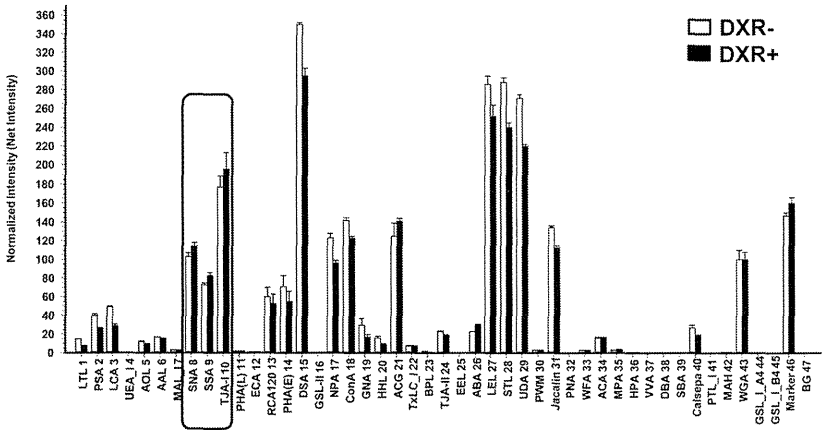

Figure 1. Lectin microarray analysis. Total cellular proteins of Huh7 cells treated with or without doxorubicin were analyzed three times using lectin microarray. Twenty-five nanogram aliquots of Cy3-labeled proteins were applied to each lectin microarray. The fluorescence intensity of each lectin was normalized to the intensity of WGA staining. All data are represented as mean ± standard deviations (SD). The Wilcoxon test was used to assess any significant differences in variables. There were significant increases in the intensities of SNA, SSA, and TJA-1 after doxorubicin treatment (DXR+) compared with the intensities in the absence of doxorubicin treatment (DXR−) ($P < 0.05$).

Table 1. Expression Profile of Sialylated Proteins in Doxorubicin-Treated Huh7 Cells, Obtained from iTRAQ Analysis

Swiss-Prot accession number	sequence	description	gene symbol	site	115/114	115/114 count	115/114 variability [%]
Q9Y4L1	VFGSQNLTTVK	hypoxia up-regulated protein 1	*HYOU1*	N515	7.137	1	
P13674	DMSDGFISNLTIQR	prolyl 4-hydroxylase subunit alpha-1	*P4HA1*	N367	4.857	1	
P11279	SGPKNMTFDLPSDATVVLNR	lysosome-associated membrane glycoprotein 1	*LAMP1*	N562, N76	3.796	1	
O60568	SAEFFNYTVR	procollagen-lysine, 2-oxoglutarate 5-dioxygenase 3	*PLOD3*	N63	2.848	1	
O60568	EQYIHENYSR	procollagen-lysine, 2-oxoglutarate 5-dioxygenase 3	*PLOD3*	N548	2.347	1	
P11142	VEIIANDQGNR	heat shock cognate 71 kDa protein	*HSPA8*	N31	2.152	1	
P16278	NNVITLNITGK	beta-galactosidase	*GLB1*	N458, N464	1.963	1	
P11279	NMTFDLPSDATVVLNR	lysosome-associated membrane glycoprotein 1	*LAMP1*	N62, N76	1.890	1	
Q92508	ELYNGTADITLR	piezo-type mechanosensitive ion channel component 1	*PIEZO1*	N2294	1.852	1	
P11279	ENTSDPSLVIAFGR	lysosome-associated membrane glycoprotein 1	*LAMP1*	N84	1.836	2	6.0
Q86VZ4	SSDNVSVTVLR	low-density lipoprotein receptor-related protein 11	*LRP11*	N291	1.806	2	8.6
P19022	SNISILR	cadherin-2	*CDH2*	N692	1.804	1	
P13473	AASTYSIDSVSFSYNTGDNTTFPDAEDK	lysosome-associated membrane glycoprotein 2	*LAMP2*	N257	1.699	1	
Q5ZPR3	TALFPDLLAQGNASLR	CD276 antigen	*CD276*	N104	1.697	1	
P11047	TLAGENQTAFEIEELNR	laminin subunit gamma-1	*LAMC1*	N1223	1.696	1	
Q5ZPR3	QLVHSFAEGQDQGSAYANR	CD276 antigen	*CD276*	N309	1.634	1	
P13473	VQPFNVTQGK	lysosome-associated membrane glycoprotein 2	*LAMP2*	N356	1.614	2	12.5
P56199	VYVYALNQTR	integrin alpha-1	*ITGA1*	N532	1.611	1	

and fixed with methanol for 10 min at −20 °C, followed by blocking with PBS containing 1% BSA for 1 h at RT. The cells were then incubated overnight at 4 °C with the mouse antifetuin-A antibody (Santa Cruz Biotechnology) and rabbit antialbumin antibody (Rockland Immunochemicals, Gilbertsville, PA, USA). Fluorescein isothiocyanate (FITC)-conjugated SSA (J-Oil Mills, Inc., Tokyo, Japan) was incubated for 2 h at RT. Primary antibody binding was detected with Alexa-488 antimouse IgG or Alexa-546 antirabbit IgG (Invitrogen). Finally, the cells were washed three times for 2 min with PBS. Staining was evaluated using confocal microscopy.

Statistical Analysis

Statistical analyses were conducted using JMP Pro 10.0 software (SAS Institute Inc., Cary, NC, USA). Variables in lectin array analyses were expressed as the mean ± standard deviation (SD). The Wilcoxon test was used to assess any significant differences in variables. Differences were considered statistically significant at $P < 0.05$.

RESULTS

Glycan Profiling of Huh7 Cells Treated with or without DXR Using Lectin Microarray

First, we determined the DXR IC_{50} concentration in Huh7 cells treated with DXR for 48 h, using the WST assay (Nacalai Tesque, Kyoto, Japan) (data not shown). Huh7 cells were treated with the IC_{50} concentration of DXR (5 μg/mL) for 48 h, and then Cy3-labeled proteins derived from these cells were subjected to lectin microarray analysis (Figure 1). Interestingly, the intensities of three sialylated glycan-recognizing lectins (SNA, SSA, and TJA-1) among 43 lectins were significantly higher in DXR-treated cells than in untreated cells. This finding is very similar to that of our previous study, which demonstrated that hepatic CSCs (CD133 and CD13 double-positive Huh7 cells) highly expressed sialylated glycans.[16] In this previous study, we also demonstrated that SSA lectin could be used as a tool for isolating CSCs. Unexpectedly, binding to the lectins PSA and LCA was slightly decreased in DXR-treated cells. Both PSA and LCA lectins recognize α1−6 core fucosylation, which is involved in carcinogenesis. Changes in the branching formation of *N*-glycans, as judged by binding to L4-PHA lectin, were not observed in Huh7 cells treated with DXR.

Sialylated Protein Expression Profile of Huh7 Cells Treated with or without DXR

To identify target glycoproteins that show increased sialylation upon DXR treatment, iTRAQ analysis was performed. Total cell lysates from Huh7 cells treated with or without DXR were trypsinized and applied to a SSA-agarose column. Subsequently, captured sialylated glycopeptides were deglycosylated with glycopeptidase F and labeled with a specific isobaric iTRAQ reagent. A total of 191 proteins were identified with this analysis. Among these, we have listed glycoproteins that showed more than 1.6-fold expression in DXR-treated Huh7 cells as compared with that in DXR-untreated Huh7 cells (Table 1).

Western Blot Analysis of Glycoprotein Listed by iTRAQ Analysis

To further verify the changes in the glycoproteins listed in Table 1, we selected four proteins [hypoxia up-regulated protein 1 (HYOU1), prolyl 4-hydroxylase subunit alpha-1 (P4HA1), lysosomal-associated membrane glycoprotein 1 (LAMP1), and LAMP2], which are known to be abundantly glycosylated and associated with cancer, for validation using Western blotting (Figure 2). The expression levels of HYOU1 and P4HA1 showed no significant differences between Huh7 cells with or without DXR treatment. This indicates that the sialylation levels of these proteins increased with DXR treatment and total protein levels were not changed. In contrast, both LAMP1 and LAMP2 protein levels were slightly increased in DXR-treated Huh7 cells.

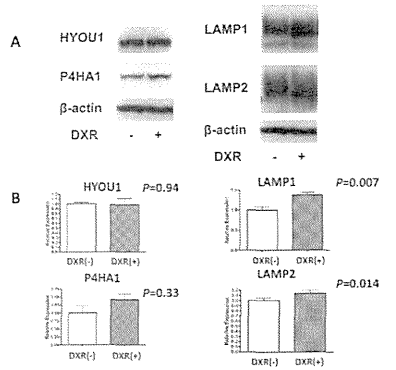

Figure 2. Western blot analyses of HYOU1, P4HA1, LAMP1, and LAMP2. (A) Twenty-five micrograms (HYOU1 and P4HA1), 10 μg (LAMP1 and β-actin), and 2.5 μg (LAMP2) of total cellular proteins were electrophoresed on 8% polyacrylamide gels, and Western blot analyses were performed. β-actin was used as the control. (B) Expression level of each protein band was determined by ImageJ64 software for three independent blots, and statistical analysis was performed by Wilcoxon test. Each result represented the mean ± SD.

Increase in Sialylation of 70 kDa Proteins in DXR-Treated Huh7 Cells

Next, we performed lectin blot analysis to determine changes in sialylation in each protein band in DXR-treated Huh7 cells. Very interestingly, dramatic increases in sialylation in approximately 70 kDa proteins were observed (Figure 3A). While other bands

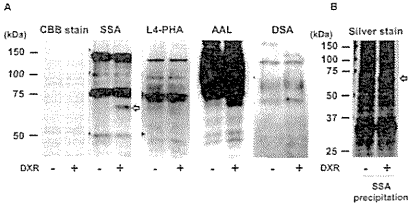

Figure 3. Lectin blot analyses and SSA precipitation of Huh7 cells treated with or without doxorubicin. (A) Lectin blot analyses using SSA, AAL, L4-PHA, and DSA. (B) Proteins were captured by SSA-agarose bead complexes, followed by 10% SDS-PAGE analysis with silver staining. The arrows indicate specifically sialylated bands. These data were results from 3−5 independent experiments.

in the SSA lectin blot were slightly increased or decreased in DXR-treated cells, the 70 kDa proteins were very prominent. Therefore, the protein levels of these 70 kDa proteins might be increased upon DXR treatment. Mechanisms that can increase sialylation in glycoproteins include increased branching, increased presence of Lewis structures, and extension of lactosamine structure repeats. L4-PHA, AAL, and DSA can recognize these glycan structures, respectively. Therefore, we examined these lectin blot analyses. The 70 kDa band was not

detected in other lectin blot analyses, although a significant increase was observed in AAL lectin blot analysis (Figure 3A). The increase in the intensity of the 70 kDa band in the DXR-treated cells in the AAL blot indicates an increased presence of Lewis structures in some glycoproteins. To capture this sialylated glycoprotein at 70 kDa, SSA precipitation was performed (Figure 3B). As shown in Figure 3B, approximately 70 kDa sialylated glycoproteins were identified using SSA-agarose precipitation followed by silver staining. Next, the 70 kDa protein spot was digested with trypsin, and the extracted peptides were analyzed using LC–MS/MS. The spectra thus acquired were searched against the Swiss-Prot database with the aid of the MASCOT search engine. In this manner, we identified five proteins as candidate sialylated glycoproteins (Table 2).

Table 2. Sialylated 70 kDa Proteins Identified by LC–MS/MS

Swiss-Prot accession no.	protein	peptide matching	protein coverage (%)
P16278	beta-galactosidase	12	11.23
P02765	alpha-2-HS-glycoprotein (fetuin-A)	8	5.45
Q02413	desmoglein-1	2	0.95
Q9NPR9	protein GPR108	2	2.03
P11279	lysosome-associated membrane glycoprotein 1	1	2.64

Evaluation of the 70 kDa Sialylated Proteins in DXR-Treated Huh7 Cells by Western Blot

To evaluate the 70 kDa sialylated proteins listed in Table 1, Western blotting was performed. Because of their large hit numbers in LC–MS/MS analysis, we focused on fetuin-A and beta-galactosidase. Although the protein expression of beta-galactosidase was slightly increased in DXR-treated Huh7 cells, the protein expression of beta-galactosidase obtained by SSA precipitation was much greater in DXR-treated Huh7 cells (Figure 4A). This result indicates that the sialylation levels of beta-galactosidase increased with DXR treatment. Next, Western blot analyses of alpha-2-HS-glycoprotein (fetuin-A) were performed. Although the protein expression of fetuin-A in total cell lysate was lower in DXR-treated Huh7 cells, the protein expression of fetuin-A obtained by SSA precipitation was significantly higher in DXR-treated Huh7 cells (Figure 4B). Furthermore, the molecular weight of fetuin-A was higher in DXR-treated Huh7 cells. These results indicate that oligosaccharide structures of fetuin-A are completely different between DXR-treated and untreated Huh7 cells. Additionally, the molecular weight of fetuin-A in the conditioned medium was almost the same between DXR-treated and untreated cells, which was consistent with the sialylated fetuin-A band (70 kDa) observed in cell lysates treated with DXR (Figure 4C). We found that sialylated fetuin (70 kDa) was barely observed in untreated cell lysate and almost all of the 70 kDa fetuin was secreted into the medium in the absence of DXR treatment. In order to determine whether the changes in molecular weight of fetuin-A were due to glycosylation/sialylation, the total cell lysates of DXR-treated and untreated Huh7 cells were incubated with 200 mU/mL neuraminidase, which specifically cleaves terminal sialic acid residues. A decrease of the molecular weight of fetuin-A was observed following neuraminidase treatment, suggesting that sialylation in fetuin-A was increased upon DXR treatment (Figure 4D). Next, to determine whether the changes in fetuin-A bands were dependent on N-glycosylation, cell lysates were treated with 20 mU/mL glycopeptidase F, which removes most complex type N-linked carbohydrates from glycoproteins. As expected, the fetuin-A band was decreased following this treatment (Figure 4D).

Localization of Fetuin-A in Huh7 Cells Treated with DXR

To examine the localization of fetuin-A in DXR-treated Huh7 cells, an immunofluorescence study was performed. Cells were stained with antifetuin-A antibody (Figure 5A,B), and anti-albumin antibody, which served as a nonglycosylated secretory protein control (Figure 5A) and SSA (Figure 5B). Although the expression of fetuin-A was lower in DXR-treated Huh7 cells than in untreated cells, colocalization of fetuin-A and albumin were observed in DXR-treated and untreated cells. In contrast, the localization of SSA changed dramatically in DXR-treated cells (Figure 5B). The localization of these signals was altered in DXR-treated cells from a perinuclear pattern to a scatter pattern in the cytoplasm. SSA and fetuin-A were not colocalized in DXR-untreated cells, but a few DXR-treated cells showed colocalization of SSA and fetuin-A (Figure 5B).

DISCUSSION

In the present study, to identify target glycoproteins for SSA lectin, we first used iTRAQ systems with SSA-agarose capture. However, the amounts of cellular proteins that could be isolated using CD133 antibody and SSA lectin were too small for proteomic analyses. Therefore, we used the anticancer drug DXR. Theoretically, treatment with DXR at its IC_{50} can concentrate CSCs. Lectin array analyses showed increased binding to SSA, SNA, and TJA-1 in DXR-treated Huh7 cells. Similar results were obtained in CD133 and CD13 double-positive CSCs derived from Huh7 cells.[16] These findings suggest that Huh7 cells treated with DXR display similar characteristics to CSCs. SSA, SNA, and TJA-1 recognize terminal α2, 6-sialic acid residues. We speculate that this increased sialylation in DXR-treated Huh7 cells might have potential benefits for the survival of anticancer drug-treated cells. To identify those glycoproteins that are targets for sialylation, iTRAQ analysis was performed. Of the 19 candidate glycoproteins we identified, concentration of HYOU1 was much greater than those of the other glycoproteins. HYOU1 plays an important role in hypoxia/ischemia and angiogenesis. HYOU1 is overexpressed in invasive breast cancer, and its overexpression appears to be associated with poor prognosis.[35] A high score in iTRAQ analyses using SSA agarose capture may indicate one of two possibilities: an increase in the glycoprotein level itself or an increase in sialic acid levels in a specific glycoprotein. Protein levels remain unchanged in the case of HYOU1 (Figure 2). Although we would have liked to perform immunoprecipitation followed by SSA lectin blotting, the antibody for immunoprecipitation was not available. We predict that sialic acid increases in HYOU1 in DXR-treated Huh7 cells. The next high score in iTRAQ analysis was that of P4HA1. P4HA1 plays a central role in collagen synthesis. P4HA1 has also been shown to be expressed in hepatocellular carcinoma tissue. In contrast, the protein expression levels of LAMP1 and LAMP2 were increased with DXR treatment. LAMP1 and LAMP2 are localized primarily in the periphery of lysosomes and are recognized as major constituents of the lysosomal membrane.[36] It is well-known that these molecules are among the most heavily glycosylated cellular proteins, with approximately 50% of their mass being carbohydrates. Therefore, these proteins could be captured by an SSA-agarose column and detected using iTRAQ analysis. Since these 4 glycoproteins are associated with cancer progression as well as metastasis, increases in sialic acid content

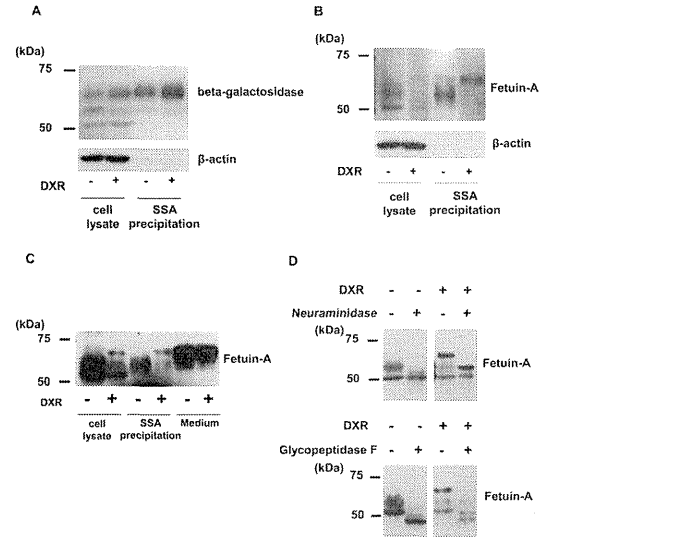

Figure 4. Evaluation of 70 kDa sialylated proteins in Huh7 cells treated with doxorubicin with Western blotting. (A) Ten micrograms of cell lysate and total cellular proteins obtained from lectin precipitation (50 μg) were electrophoresed on 8% acrylamide gels, and Western blot analyses of beta-galactosidase were performed. (B) Western blotting analysis of fetuin-A was performed. (C) Western blotting analysis of fetuin-A from Huh7 cell lysates (30 μg) and conditioned media (1 μL) in the presence or absence of DXR treatment. (D) Cell lysates were treated with neuraminidase or glycopeptidase F at 37 °C overnight. The lysates were then subjected to 8% SDS-PAGE analysis. These data were results from 3 independent experiments.

in these proteins can change biological characteristics, including cancer stemness.

Next, we conducted an SSA lectin blot analysis to determine total/partial increases in sialic acid content in DXR-treated Huh7 cells. Surprisingly, proteins approximately 70 kDa in mass were specifically sialylated. From LC–MS/MS analyses, we identified five proteins that were not identified by iTRAQ analysis, with the exception of LAMP1. Fetuin-A (predicted molecular weight: 38 kDa), GPR108 (predicted molecular weight: 60 kDa), LAMP1 (predicted molecular weight: 45 kDa), and LAMP2 (predicted molecular weight: 45 kDa) are abundantly glycosylated. In our study, 70 kDa fetuin-A was heavily sialylated. Therefore, the band sizes of fetuin-A, GPR108, LAMP1, and LAMP2 were heavier than the predicted molecular weights. In addition, the predicted size of beta-galactosidase is about 116 kDa, but the alternatively spliced variant of beta-galactosidase was reported to be about 67 kDa.[37] Desmoglein-1 (predicted molecular weight: 112 kDa) would be cleaved by DXR-activated proteases. The reason why these proteins were not identified by iTRAQ is likely due to the analysis method of iTRAQ. Because proteins are cleaved into peptides in iTRAQ analysis, the steric structures of each protein is not reflected in iTRAQ analysis. In contrast, the steric structures of each protein and the site of *N*-glycan attachment are necessary in SSA precipitation analysis. These differences between iTRAQ and SSA precipitation are likely the reason for the different results seen in our study.

In LC–MS/MS analysis, we focused on beta-galactosidase and fetuin-A because of their predominantly large hit numbers. Beta-galactosidase (lysosomal hydrolase) cleaves the terminal beta-galactose from glycoconjugates. It is reported that anticancer drug treatment induces a senescence-like phenotype, and senescent cells are characterized by the appearance of senescence-associated beta-galactosidase.[38] Therefore, increases in sialic acid in beta-galactosidase in DXR-treated Huh7 cells are very interesting. Another glycoprotein, identified as a 70 kDa sialylated glycoprotein, was fetuin-A. Fetuin-A is well-known as a heavily sialylated glycoprotein with both N-linked and O-linked carbohydrate side chains.[39,40] Although various previous reports have discussed the biological functions of fetuin-A,[41,42] no studies have demonstrated differences in fetuin-A functions due to glycosylation differences. Asialofetuin-A is well-known to bind easily to galectin-3, while sialylated fetuin (sialofetuin) is reported to have no binding ability to galectin-3.[43,44] These biological differences would contribute to the functional diversity of variously glycosylated fetuin-A.

Neuraminidase treatment decreases the molecular weight of fetuin-A in DXR-treated Huh7 cells, and the lowered molecular weight was consistent with that of fetuin-A in DXR-untreated Huh7 cells, suggesting that fetuin-A was heavily sialylated in DXR-treated Huh7 cells. The question arises as to why this sialylated fetuin-A was not secreted into the conditioned medium. Therefore, we performed immunocytochemical analysis using confocal microscopy. Most of the fetuin-A was colocalized with albumin in DXR-treated cells compared to untreated cells, indicating that the secreted proteins were in the same endosome as during DXR treatment. A previous study

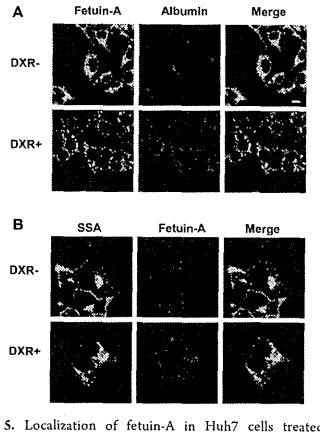

Figure 5. Localization of fetuin-A in Huh7 cells treated with doxorubicin. Immunocytochemical analyses were performed in Huh7 cells treated with or without DXR. After fixation of the cells, staining signals were visualized by laser scanning confocal microscopy. (A) Fetuin-A was visualized by Alexa-488-labeled immunostaining (green), albumin was visualized by Alexa-546-labeled immunostaining (red). (B) SSA was visualized by FITC labeling (green), and fetuin-A was visualized by Alexa-546-labeled immunostaining (red). The magnification is ×120. The bar indicates 10 μm. These data were results from 3 independent experiments.

showed that DXR induced apoptosis at a high dose (IC_{90}) but induced autophagy at a low dose (IC_{50}).[45] However, fetuin-A was not located in either the lysosome or the autophagosome (data not shown). Next we examined immunostaining of SSA to detect sialylated proteins. Surprisingly, SSA staining was dramatically changed, and a few cells showed colocalization of fetuin-A and SSA in DXR-treated cells. These results indicate that a small amount of sialylated fetuin-A remained inside the cell in DXR-treated cells. In general, fetuin-A is known as a highly sialylated serum protein.[46] Most sialylated fetuin-A might be promptly secreted to the conditioned medium (Figure 4C). In contrast, a small amount of sialylated fetuin-A remained inside the cell in DXR-treated cells. Further studies should be performed using sialyltransferase knockout or knockdown cells to evaluate the relationship between sialylation and the localization of glycoproteins, especially that of fetuin-A in anticancer drug treated cells. Since sialylation is a glycomarker for stem cells,[16,47] changes in the localization of sialylated proteins in CSCs might be involved in stem cell biology.

■ ASSOCIATED CONTENT

Supporting Information

Proliferation of CD133 positive Huh7 cells (SSA positive (+) or negative (−)) under 5-FU treatment. Raw data of MS/MS analysis. List of the glycoproteins identified in iTRAQ analysis. This material is available free of charge via the Internet at http://pubs.acs.org.

■ AUTHOR INFORMATION

Corresponding Author

*(E.M.) Tel/Fax: +81-6-6879-2590. E-mail: emiyoshi@sahs.med.osaka-u.ac.jp.

Notes

The authors declare no competing financial interest.

■ ACKNOWLEDGMENTS

This study was supported by a Grant-in-Aid for Scientific Research (A), No. 21249038, from the Japan Society for the Promotion of Science, and partially supported as a research program of the Project for Development of Innovative Research on Cancer Therapeutics (P-Direct), Ministry of Education, Culture, Sports, Science and Technology of Japan.

■ ABBREVIATIONS

CSCs, cancer stem cells; DXR, doxorubicin; SSA, *Sambucus sieboldiana* agglutinin; SNA, *Sambucus nigra* lectin; TJA-1, *Tricosanthes japonica* agglutinin-1; PSA, *Pisum sativum* agglutinin; LCA, *Lens culinaris* agglutinin; WGA, Wheat germ agglutinin; L4-PHA, *Leukoagglutinating phytohemagglutinin*; AAL, *Aleuria aurantia* lectin; DSA, *Datura stramonium agglutinin*; iTRAQ, isobaric tags for relative and absolute quantitation; HYOU1, hypoxia up-regulated protein 1; P4HA1, prolyl 4-hydroxylase subunit alpha-1; LAMP1, lysosomal-associated membrane glycoprotein 1

■ REFERENCES

(1) Reya, T.; Morrison, S. J.; Clarke, M. F.; Weissman, I. L. Stem cells, cancer, and cancer stem cells. *Nature* **2001**, *414* (6859), 105−11.
(2) Ailles, L. E.; Weissman, I. L. Cancer stem cells in solid tumors. *Curr. Opin. Biotechnol.* **2007**, *18* (5), 460−6.
(3) Mertins, S. D. Cancer stem cells: a systems biology view of their role in prognosis and therapy. *Anticancer Drugs* **2014**, *25* (4), 353−67.
(4) Dean, M.; Fojo, T.; Bates, S. Tumour stem cells and drug resistance. *Nat. Rev. Cancer* **2005**, *5* (4), 275−84.
(5) Bao, S.; Wu, Q.; McLendon, R. E.; Hao, Y.; Shi, Q.; Hjelmeland, A. B.; Dewhirst, M. W.; Bigner, D. D.; Rich, J. N. Glioma stem cells promote radioresistance by preferential activation of the DNA damage response. *Nature* **2006**, *444* (7120), 756−60.
(6) Malik, B.; Nie, D. Cancer stem cells and resistance to chemo and radio therapy. *Front. Biosci., Elite Ed.* **2012**, *4*, 2142−9.
(7) Baumann, M.; Krause, M.; Thames, H.; Trott, K.; Zips, D. Cancer stem cells and radiotherapy. *Int. J. Radiat. Biol.* **2009**, *85* (5), 391−402.
(8) Haraguchi, N.; Ishii, H.; Mimori, K.; Tanaka, F.; Ohkuma, M.; Kim, H. M.; Akita, H.; Takiuchi, D.; Hatano, H.; Nagano, H.; Barnard, G. F.; Doki, Y.; Mori, M. CD13 is a therapeutic target in human liver cancer stem cells. *J. Clin. Invest.* **2010**, *120* (9), 3326−39.
(9) Zhu, Z.; Hao, X.; Yan, M.; Yao, M.; Ge, C.; Gu, J.; Li, J. Cancer stem/progenitor cells are highly enriched in CD133+CD44+ population in hepatocellular carcinoma. *Int. J. Cancer* **2010**, *126* (9), 2067−78.
(10) Yang, Z. F.; Ho, D. W.; Ng, M. N.; Lau, C. K.; Yu, W. C.; Ngai, P.; Chu, P. W.; Lam, C. T.; Poon, R. T.; Fan, S. T. Significance of CD90+ cancer stem cells in human liver cancer. *Cancer Cell* **2008**, *13* (2), 153−66.
(11) Al-Hajj, M.; Wicha, M. S.; Benito-Hernandez, A.; Morrison, S. J.; Clarke, M. F. Prospective identification of tumorigenic breast cancer cells. *Proc. Natl. Acad. Sci. U.S.A.* **2003**, *100* (7), 3983−8.
(12) Kojima, K.; Musch, M. W.; Ren, H.; Boone, D. L.; Hendrickson, B. A.; Ma, A.; Chang, E. B. Enteric flora and lymphocyte-derived cytokines determine expression of heat shock proteins in mouse colonic epithelial cells. *Gastroenterology* **2003**, *124* (5), 1395−407.
(13) Ding, W.; Mouzaki, M.; You, H.; Laird, J. C.; Mato, J.; Lu, S. C.; Rountree, C. B. CD133+ liver cancer stem cells from methionine adenosyl transferase 1A-deficient mice demonstrate resistance to transforming growth factor (TGF)-beta-induced apoptosis. *Hepatology* **2009**, *49* (4), 1277−86.
(14) Fuster, M. M.; Esko, J. D. The sweet and sour of cancer: glycans as novel therapeutic targets. *Nat. Rev. Cancer* **2005**, *5* (7), 526−42.

(15) Haltiwanger, R. S.; Lowe, J. B. Role of glycosylation in development. *Annu. Rev. Biochem.* **2004**, *73*, 491−537.
(16) Moriwaki, K.; Okudo, K.; Haraguchi, N.; Takeishi, S.; Sawaki, H.; Narimatsu, H.; Tanemura, M.; Ishii, H.; Mori, M.; Miyoshi, E. Combination use of anti-CD133 antibody and SSA lectin can effectively enrich cells with high tumorigenicity. *Cancer Sci.* **2011**, *102* (6), 1164−70.
(17) Varki, A. Sialic acids in human health and disease. *Trends Mol. Med.* **2008**, *14* (8), 351−60.
(18) Yogeeswaran, G.; Salk, P. L. Metastatic potential is positively correlated with cell surface sialylation of cultured murine tumor cell lines. *Science* **1981**, *212* (4502), 1514−6.
(19) Fogel, M.; Altevogt, P.; Schirrmacher, V. Metastatic potential severely altered by changes in tumor cell adhesiveness and cell-surface sialylation. *J. Exp. Med.* **1983**, *157* (1), 371−6.
(20) Passaniti, A.; Hart, G. W. Cell surface sialylation and tumor metastasis. Metastatic potential of B16 melanoma variants correlates with their relative numbers of specific penultimate oligosaccharide structures. *J. Biol. Chem.* **1988**, *263* (16), 7591−603.
(21) Cui, H.; Lin, Y.; Yue, L.; Zhao, X.; Liu, J. Differential expression of the alpha2,3-sialic acid residues in breast cancer is associated with metastatic potential. *Oncol. Rep.* **2011**, *25* (5), 1365−71.
(22) Babal, P.; Janega, P.; Cerna, A.; Kholova, I.; Brabencova, E. Neoplastic transformation of the thyroid gland is accompanied by changes in cellular sialylation. *Acta Histochem.* **2006**, *108* (2), 133−40.
(23) Sethi, M. K.; Thaysen-Andersen, M.; Smith, J. T.; Baker, M. S.; Packer, N. H.; Hancock, W. S.; Fanayan, S. Comparative N-glycan profiling of colorectal cancer cell lines reveals unique bisecting GlcNAc and alpha-2,3-linked sialic acid determinants are associated with membrane proteins of the more metastatic/aggressive cell lines. *J. Proteome Res.* **2014**, *13* (1), 277−88.
(24) Lanctot, P. M.; Gage, F. H.; Varki, A. P. The glycans of stem cells. *Curr. Opin. Chem. Biol.* **2007**, *11* (4), 373−80.
(25) Taniguchi, N.; Ekuni, A.; Ko, J. H.; Miyoshi, E.; Ikeda, Y.; Ihara, Y.; Nishikawa, A.; Honke, K.; Takahashi, M. A glycomic approach to the identification and characterization of glycoprotein function in cells transfected with glycosyltransferase genes. *Proteomics* **2001**, *1* (2), 239−47.
(26) Hermann, P. C.; Huber, S. L.; Herrler, T.; Aicher, A.; Ellwart, J. W.; Guba, M.; Bruns, C. J.; Heeschen, C. Distinct populations of cancer stem cells determine tumor growth and metastatic activity in human pancreatic cancer. *Cell Stem Cell* **2007**, *1* (3), 313−23.
(27) Ross, P. L.; Huang, Y. N.; Marchese, J. N.; Williamson, B.; Parker, K.; Hattan, S.; Khainovski, N.; Pillai, S.; Dey, S.; Daniels, S.; Purkayastha, S.; Juhasz, P.; Martin, S.; Bartlet-Jones, M.; He, F.; Jacobson, A.; Pappin, D. J. Multiplexed protein quantitation in Saccharomyces cerevisiae using amine-reactive isobaric tagging reagents. *Mol. Cell Proteomics* **2004**, *3* (12), 1154−69.
(28) Zieske, L. R. A perspective on the use of iTRAQ reagent technology for protein complex and profiling studies. *J. Exp. Bot* **2006**, *57* (7), 1501−8.
(29) Kuno, A.; Uchiyama, N.; Koseki-Kuno, S.; Ebe, Y.; Takashima, S.; Yamada, M.; Hirabayashi, J. Evanescent-field fluorescence-assisted lectin microarray: a new strategy for glycan profiling. *Nat. Methods* **2005**, *2* (11), 851−6.
(30) Serada, S.; Fujimoto, M.; Ogata, A.; Terabe, F.; Hirano, T.; Iijima, H.; Shinzaki, S.; Nishikawa, T.; Ohkawara, T.; Iwahori, K.; Ohguro, N.; Kishimoto, T.; Naka, T. iTRAQ-based proteomic identification of leucine-rich alpha-2 glycoprotein as a novel inflammatory biomarker in autoimmune diseases. *Ann. Rheum. Dis.* **2010**, *69* (4), 770−4.
(31) Serada, S.; Fujimoto, M.; Takahashi, T.; He, P.; Hayashi, A.; Tanaka, T.; Hagihara, K.; Yamadori, T.; Mochizuki, M.; Norioka, N.; Norioka, S.; Kawase, I.; Naka, T. Proteomic analysis of autoantigens associated with systemic lupus erythematosus: Anti-aldolase A antibody as a potential marker of lupus nephritis. *Proteomics Clin. Appl.* **2007**, *1* (2), 185−91.
(32) He, P.; Naka, T.; Serada, S.; Fujimoto, M.; Tanaka, T.; Hashimoto, S.; Shima, Y.; Yamadori, T.; Suzuki, H.; Hirashima, T.; Matsui, K.; Shiono, H.; Okumura, M.; Nishida, T.; Tachibana, I.; Norioka, N.; Norioka, S.; Kawase, I. Proteomics-based identification of alpha-enolase as a tumor antigen in non-small lung cancer. *Cancer Sci.* **2007**, *98* (8), 1234−40.
(33) Shevchenko, A.; Wilm, M.; Vorm, O.; Mann, M. Mass spectrometric sequencing of proteins silver-stained polyacrylamide gels. *Anal. Chem.* **1996**, *68* (5), 850−8.
(34) Kuwamoto, K.; Takeda, Y.; Shirai, A.; Nakagawa, T.; Takeishi, S.; Ihara, S.; Miyamoto, Y.; Shinzaki, S.; Ko, J. H.; Miyoshi, E. Identification of various types of alpha2-HS glycoprotein in sera of patients with pancreatic cancer: Possible implication in resistance to protease treatment. *Mol. Med. Rep* **2010**, *3* (4), 651−6.
(35) Stojadinovic, A.; Hooke, J. A.; Shriver, C. D.; Nissan, A.; Kovatich, A. J.; Kao, T. C.; Ponniah, S.; Peoples, G. E.; Moroni, M. HYOU1/Orp150 expression in breast cancer. *Med. Sci. Monit* **2007**, *13* (11), BR231−239.
(36) Fukuda, M.; Viitala, J.; Matteson, J.; Carlsson, S. R. Cloning of cDNAs encoding human lysosomal membrane glycoproteins, h-lamp-1 and h-lamp-2. Comparison of their deduced amino acid sequences. *J. Biol. Chem.* **1988**, *263* (35), 18920−8.
(37) Privitera, S.; Prody, C. A.; Callahan, J. W.; Hinek, A. The 67-kDa enzymatically inactive alternatively spliced variant of beta-galactosidase is identical to the elastin/laminin-binding protein. *J. Biol. Chem.* **1998**, *273* (11), 6319−26.
(38) Eom, Y. W.; Kim, M. A.; Park, S. S.; Goo, M. J.; Kwon, H. J.; Sohn, S.; Kim, W. H.; Yoon, G.; Choi, K. S. Two distinct modes of cell death induced by doxorubicin: apoptosis and cell death through mitotic catastrophe accompanied by senescence-like phenotype. *Oncogene* **2005**, *24* (30), 4765−77.
(39) Hayase, T.; Rice, K. G.; Dziegielewska, K. M.; Kuhlenschmidt, M.; Reilly, T.; Lee, Y. C. Comparison of N-glycosides of fetuins from different species and human alpha 2-HS-glycoprotein. *Biochemistry* **1992**, *31* (20), 4915−21.
(40) Edge, A. S.; Spiro, R. G. Presence of an O-glycosidically linked hexasaccharide in fetuin. *J. Biol. Chem.* **1987**, *262* (33), 16135−41.
(41) Stefan, N.; Haring, H. U. The role of hepatokines in metabolism. *Nat. Rev. Endocrinol.* **2013**, *9* (3), 144−52.
(42) Wang, H.; Sama, A. E. Anti-inflammatory role of fetuin-A in injury and infection. *Curr. Mol. Med.* **2012**, *12* (5), 625−33.
(43) Inohara, H.; Raz, A. Identification of human melanoma cellular and secreted ligands for galectin-3. *Biochem. Biophys. Res. Commun.* **1994**, *201* (3), 1366−75.
(44) von Mach, T.; Carlsson, M. C.; Straube, T.; Nilsson, U.; Leffler, H.; Jacob, R. Ligand binding and complex formation of galectin-3 is modulated by pH variations. *Biochem. J.* **2014**, *457* (1), 107−15.
(45) Akar, U.; Chaves-Reyez, A.; Barria, M.; Tari, A.; Sanguino, A.; Kondo, Y.; Kondo, S.; Arun, B.; Lopez-Berestein, G.; Ozpolat, B. Silencing of Bcl-2 expression by small interfering RNA induces autophagic cell death in MCF-7 breast cancer cells. *Autophagy* **2008**, *4* (5), 669−79.
(46) Ohnishi, T.; Nakamura, O.; Ozawa, M.; Arakaki, N.; Muramatsu, T.; Daikuhara, Y. Molecular cloning and sequence analysis of cDNA for a 59 kD bone sialoprotein of the rat: demonstration that it is a counterpart of human alpha 2-HS glycoprotein and bovine fetuin. *J. Bone Miner. Res.* **1993**, *8* (3), 367−77.
(47) Martin, M. J.; Muotri, A.; Gage, F.; Varki, A. Human embryonic stem cells express an immunogenic nonhuman sialic acid. *Nat. Med.* **2005**, *11* (2), 228−32.

Annexin A4 induces platinum resistance in a chloride-and calcium-dependent manner

Akiko Morimoto[1,2], Satoshi Serada[2], Takayuki Enomoto[3], Ayako Kim[2], Shinya Matsuzaki[1], Tsuyoshi Takahashi[2,4], Yutaka Ueda[1], Kiyoshi Yoshino[1], Masami Fujita[1], Minoru Fujimoto[2], Tadashi Kimura[1] and Tetsuji Naka[2]

[1] Department of Obstetrics and Gynecology, Osaka University Graduate School of Medicine, Japan

[2] Laboratory for Immune Signals, National Institute of Biomedical Innovation, Japan

[3] Department of Obstetrics and Gynecology, Niigata University Medical School, Japan

[4] Department of Surgery, Osaka University Graduate School of Medicine, Japan

Correspondence to: *Tetsuji Naka* , ***email***: *tnaka@nibio.go.jp*

Keywords: Annexin A4; platinum resistance; annexin repeat; chloride ion

Received: *April 04, 2014* ***Accepted***: *August 03, 2014* ***Published***: *August 04, 2014*

ABSTRACT

Platinum resistance has long been a major issue in the treatment of various cancers. We previously reported that enhanced annexin A4 (ANXA4) expression, a Ca^{2+}-regulated phospholipid-binding protein, induces chemoresistance to platinum-based drugs. In this study, we investigated the role of annexin repeats, a conserved structure of all the annexin family, responsible for platinum-resistance as well as the effect of knockdown of ANXA4. ANXA4 knockdown increased sensitivity to platinum-based drugs both *in vitro* and *in vivo*. To identify the domain responsible for chemoresistance, ANXA4 deletion mutants were constructed by deleting annexin repeats one by one from the C terminus. Platinum resistance was induced both *in vitro* and *in vivo* in cells expressing either full-length ANXA4 or the deletion mutants, containing at least one intact annexin repeat. However, cells expressing the mutant without any calcium-binding sites in the annexin repeated sequence, which is essential for ANXA4 translocation from the cytosol to plasma membrane, failed to acquire platinum resistance. After cisplatin treatment, the intracellular chloride ion concentration, whose channel is partly regulated by ANXA4, significantly increased in the platinum-resistant cells. These findings indicate that the calcium-binding site in the annexin repeat induces chemoresistance to the platinum-based drug by elevating the intracellular chloride concentration.

INTRODUCTION

Since cisplatin was first introduced as an anticancer drug in the 1970s [1], various platinum-based drugs have been developed and widely used not only against gynecological but also against other cancers, including lung, colorectal, testicular, prostate and bladder cancer [2-6]. Although these platinum-based drugs have significantly contributed to improve survival rates, chemoresistance to these drugs has become a major problem in recent years [7-9]. It has now been elucidated that the mechanism of platinum resistance is mediated by reduced platinum accumulation, increased platinum detoxification, increased repair of platinum–DNA adducts and inhibited apoptosis [10-12]. Several proteins have been reported to be candidate factors such as copper transporters: CTR1[13], ATP7A and ATP7B[14-17]; multidrug resistance protein 2 (MRP2) [18-20]; glutathione S-transferase enzyme π (GSTπ) [21]; excision cross-complementing gene 1 (ERCC1) [22]; receptor-interacting protein 1 (RIP1) [23]; microRNAs [24-26]; and p53 [27]. In contrast, there are still several proteins related to platinum resistance without a full understanding of how these proteins help cells to confer platinum-based drugs.

We recently reported that annexin A4 (ANXA4) is overexpressed in ovarian clear cell carcinoma and induces chemoresistance to platinum-based drugs [28]. Annexins are calcium-regulated and negatively charged phospholipid membrane-binding proteins. The basic structure of annexins consists of 2 major domains: a conserved structural element called an annexin repeat, a segment of 70 amino acid residues at the C terminus, and the N-terminal region unique for a given member of the family and determining individual annexin properties *in vivo*. The annexin repeat possesses the calcium and membrane binding sites and is responsible for mediating the canonical membrane binding properties [29]. These domains in ANXA4 are surrounded by relatively short amino and carboxy termini that do not have any known function [30]. ANXA4 is involved in membrane permeability, exocytosis and regulation of chloride channels in a calcium-dependent manner [29, 31-33]. ANXA4 is almost exclusively expressed in epithelial cells [34]. With regard to cancer, ANXA4 overexpression has been reported in various tumours, such as lung, gastric, colorectal, renal, pancreatic, ovarian and prostate cancer [28, 35-39] and is associated with tumour invasiveness, metastasis and chemoresistance [37, 40]. Moreover, ANXA4 has been shown to be associated with resistance to platinum-based drugs [28, 41-43].

ANXA4-induced platinum resistance appears to be mediated in part by the increased extracellular efflux of platinum mediated by the copper transporter ATP7A[28, 44]. Another mechanism of ANXA4-induced chemoresistance is the modulation of NF-κB transcriptional activity [45]. ANXA4 suppresses NF-κB transcriptional activity through interaction with the p50 subunit in a calcium-dependent manner; ANXA4 causes resistance to apoptosis induction by etoposide.

While ANXA4 prominently associated with chemoresistance, the functional domain of ANXA4 remains unclear. Therefore, to clarify the functional domain of ANXA4 is required to understand detailed mechanisms of the chemoresistance induced by ANXA4 and also overcome chemoresistance. In this study, focusing on platinum resistance, we aimed to identify the ANXA4 domain relevant to chemoresistance with regard to its structure as well as to test whether knockdown of ANXA4 expression could improve platinum resistance. Our data showed that the annexin repeat plays an important role in platinum resistance induced by ANXA4, which occurs in a calcium-dependent manner.

RESULTS

Establishment of ANXA4 knockdown RMG-I cells

To create cell lines with a stable ANXA4 knockdown, we analysed ANXA4 expression in ovarian cancer cells using western blotting. ANXA4 expression was strong in clear cell carcinoma cell lines (OVTOKO, OVISE and RMG-I) compared with serous adenocarcinoma cell lines (A2780, OVCAR3 and OVSAHO) and a mucinous adenocarcinoma cell line (MCAS; Fig. 1A). To see whether blocking ANXA4 expression was a valid chemosensitising strategy for ovarian clear cell carcinoma treatment, ANXA4 was stably suppressed using an ANXA4 shRNA plasmid. We established RMG-I-Y4 and R5 cell clones as well as RMG-I NC7 cell clones transfected with the empty vector as a control. Compared with RMG-I NC7 and untransfected control parent RMG-I cells, ANXA4 expression was markedly down-regulated at the protein level in RMG-I-Y4 and RMG-I-R5 cells (Fig. 1B). In the absence of any drug treatment, the growth rate among the 4 cell lines was similar *in vitro* (data not shown).

Knockdown of ANXA4 expression enhances sensitivity to cisplatin and carboplatin

The sensitivity to cisplatin and carboplatin was assessed in the 3 RMG-I clones NC7, R5 and Y4. Compared with the IC_{50} for cisplatin in NC7 cells, IC_{50} was significantly decreased in Y4 cells and R5 cells ($p < 0.01$; Fig. 1C, left panel). Similarly, IC_{50} for carboplatin significantly decreased in Y4 cells and R5 cells compared with NC7 cells ($p < 0.01$; Fig. 1C, right panel). IC_{50} for cisplatin and carboplatin decreased approximately 2-fold because of the knockdown of ANXA4 expression.

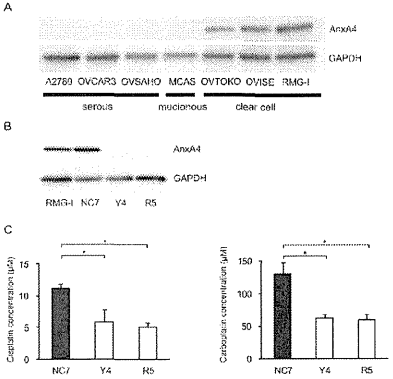

Fig.1: Knockdown of ANXA4 expression attenuates platinum resistance. (A) ANXA4 expression in indicated ovarian cancer cell lines and (B) established ANXA4 knockdown RMG-I cells (R5 and Y4) was confirmed using Western blotting. (C) IC_{50} for both cisplatin and carboplatin was significantly reduced in R5 and Y4 cells compared with NC7 cells. Data are presented as mean ± SD (*$p < 0.01$).

Suppression of ANXA4 expression improves platinum sensitivity *in vivo*

To determine whether ANXA4 knockdown in clear cell carcinoma cells improved platinum sensitivity *in vivo*, NC7 and Y4 cells were subcutaneously injected in ICR *nu/nu* mice. One week after inoculation with the tumour cells, the mice were randomised into 2 groups and received cisplatin or PBS *i.p.* twice a week for 4 weeks. The tumour growth rate in the absence of drugs was similar for both cell lines (Figs. 2A and 2B). Cisplatin treatment had very little effect on NC7 cells (Fig. 2A), but tumour volume markedly decreased in Y4 cells (Fig. 2B). Cisplatin treatment significantly decreased tumour growth in Y4 cells (87.4 ± 1.8%) compared with NC7 cells (-1.1 ± 18.0%; $p < 0.01$; Fig. 2C). These results showed that ANXA4 knockdown in the RMG-I cell line significantly attenuated resistance to cisplatin *in vivo*.

The annexin repeat domain is required for the platinum drug resistance

To identify a possible resistance-related domain within the annexin repeated sequence of ANXA4, we constructed 3 deletion mutants by deleting the annexin repeats one by one from the C-terminal region. Figure 3A shows the structure of each deletion mutant. Full-length ANXA4, 3 ANXA4 deletion mutants or the empty vector were transfected into NUGC3 cells, whose endogenous ANXA4 expression is relatively low (Supplementary Fig. S1). Therefore, we established cell lines stably overexpressing full-length ANXA4 (FL-22), each ANXA4 deletion mutant (R3-6, R2-13 or R1-12) or the empty vector (NC-14). Expression of each ANXA4 deletion mutant was confirmed using Western blotting (Fig. 3B).

Subsequently, the sensitivity to the platinum-based drugs cisplatin and carboplatin was assessed. Cells transfected with full-length ANXA4 and the 3 deletion ANXA4 mutants were significantly more resistant to both cisplatin and carboplatin compared with control cells, approximately with a 1.7- to 2.2-fold increase in IC_{50} for cisplatin ($p < 0.01$) and a 1.4- to 1.7-fold increase in IC_{50} for carboplatin ($p < 0.05$; Fig. 3C).

To test whether these deletion mutants induce platinum resistance through regulating cellular drug concentration as previously reported [28], we quantitated the intracellular platinum content of each deletion mutant-transfected cell clone after cisplatin treatment, which is one of the most representative platinum drugs. Platinum accumulation was significantly reduced in cells overexpressing either full-length ANXA4 or any of the 3

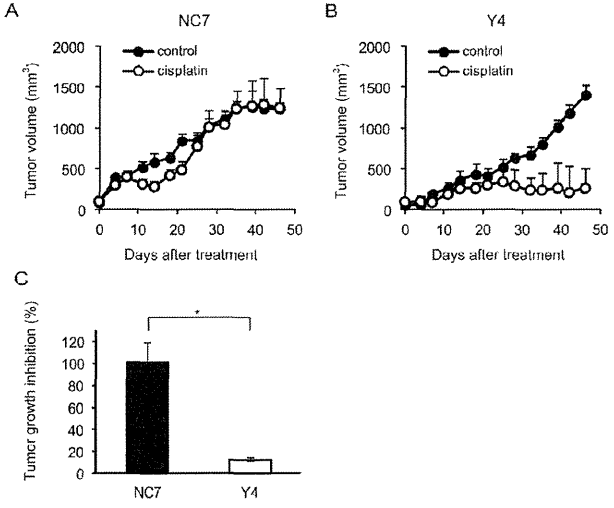

Fig.2: ANXA4 knockdown cells show enhanced sensitivity to cisplatin *in vivo*. Female ICR *nu/nu* mice were subcutaneously inoculated with RMG-I NC7 or Y4 cells and given PBS (control group: *filled circles*) or cisplatin i.p. (3 mg/kg; treatment group: *open circles*) twice weekly for 4 weeks (n = 6 per group). Growth curves of NC7 tumours (A) and Y4 tumours (B). The mean volume (points) ± SE (bars) is shown. (C) Comparison of the cisplatin-induced growth inhibition of tumours 46 days after treatment among NC7 and Y4 tumours. The average (columns) ± SE (bars) are shown (*$p < 0.01$).

deletion mutants compared with NC-14 cells regardless of the incubation time after cisplatin exposure (Fig. 3D). These results suggested that the decreased intracellular platinum contents were associated with platinum resistance of the cells transfected with ANXA4 full length and each deletion mutant.

The calcium-binding site of the annexin repeat is responsible for platinum resistance

As specified above, platinum resistance was enhanced in cells overexpressing ANXA4 deletion mutants, which contained at least 1 intact annexin repeat. Thus, to assess whether the calcium-binding site of the annexin repeat sequence was involved in chemoresistance, another deletion mutant, R1(E70A) was constructed. Within the annexin repeat next to the N-terminal region, the 70th amino acid, glutamic acid, was responsible for the calcium-dependent activity of ANXA4 [30]. Accordingly, at this site, the point mutation variant of R1, R1(E70A), loses the function of its calcium-binding site (Fig. 4A). Similar to other deletion mutants, R1(E70A) was transfected into NUGC3 cells and designated R1(E70A)-95. Western blotting revealed that R1-12 had the same molecular weight as R1(E70A)-95 (Fig. 4B). R1(E70A)-95 did not induce resistance to either cisplatin or carboplatin (Fig. 4C). Moreover, the intracellular platinum content of R1(E70A)-95-transfected cells did not decrease compared with that of NC-14 cells after 0 hr

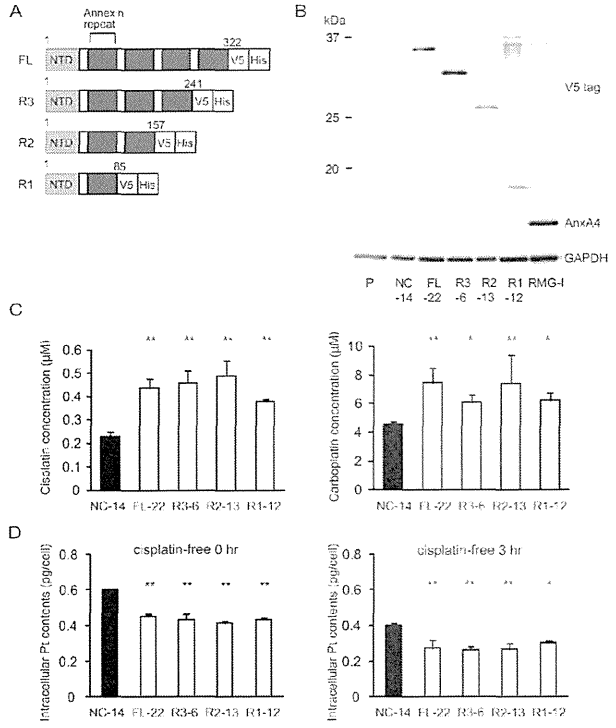

Fig.3: Annexin repeat domain is required for the platinum drug resistance. (A) A structural map of ANXA4 and 3 deletion mutant proteins. Annexin repeats were deleted one by one from the C-terminal site. (B) Established deletion mutant cells together with parent cells, control cells and RMG-I as a positive control were confirmed using Western blotting. (C) Compared with NC-14 cells, IC_{50} for both cisplatin and carboplatin was significantly increased in FL-22 and all other mutant cells. (D) Intracellular platinum accumulation after treatment with 100 μM cisplatin for 60 min with or without additional 3 hr of incubation in cisplatin-free medium. Data are presented as mean ± SD (*$p < 0.05$, **$p < 0.01$).

or 3 hr of additional incubation in cisplatin-free medium (Fig. 4D). According to the above results, the platinum resistance of ANXA4 seemed to be related to the calcium-binding site of the annexin repeat next to the N-terminal domain.

The calcium-binding site of the annexin repeated sequence is required for the resistance to platinum-based drugs *in vivo*

To determine whether the annexin deletion mutants of ANXA4 influenced the sensitivity to cisplatin *in vivo*, we inoculated ICR *nu/nu* mice with NC-14, FL-22, R1-12 or R1(E70A)-95 cells. Mice in each group were randomised into 2 subgroups and received either cisplatin at 3 mg/(kg·d) or PBS *i.p.* once a week for 3 weeks. Cisplatin markedly decreased tumour volume in mice injected with NC-14 and R1(E70A)-95 cells, whereas the treatment effect was relatively smaller in mice injected with FL-22 and R1-12 cells (Fig. 5A). Consistent with the tumour volume, tumour growth was significantly inhibited by cisplatin in mice inoculated with NC-14 (96.5 ± 1.3%) and R1(E70A)-95 cells (87.8 ± 11.4%) compared with those injected with FL-22 (48.5 ± 11.7%) and R1-12 cells (37.7 ± 9.8%; $p < 0.01$; Fig. 5B). These *in vivo* results

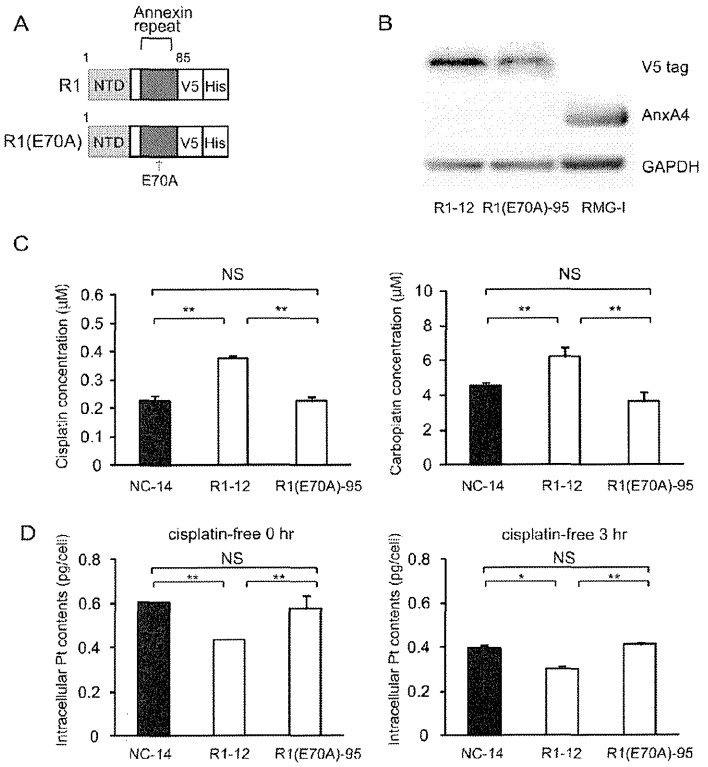

Fig.4: The calcium-binding site of the annexin repeat is responsible for induction of the platinum resistance. (A) A structural map of R1 and R1(E70A) variants without a function for the calcium-binding site. (B) Western blotting confirmed the mutant established cell lines. (C) Unlike R1-12, the R1(E70A)-95 cell clone was not resistant to either cisplatin or carboplatin. (D) Intracellular platinum accumulation in R1(E70A) cells was the same as in NC14 cells both with or without additional 3 hr of incubation in cisplatin-free medium. Data are presented as mean ± SD (*$p < 0.05$, **$p < 0.01$).

were consistent with those obtained *in vitro*.

Increase of the intracellular chloride concentration is related to cisplatin resistance

To elucidate the molecular mechanisms of chemoresistance induced by ANXA4, we focused on the chloride channel because one of the functions of ANXA4 is inhibition of calcium-dependent chloride conductance[32]. According to the literature, treatment with cisplatin induces an increase of the intracellular Ca^{2+} concentration [46], which is an important ion for the phospholipid membrane-binding activity of ANXA4. In contrast, cisplatin exposure also induces an elevation of the intracellular chloride concentration: $[Cl^-]_i$ [47]. Elevation of $[Cl^-]_i$ has been shown to prevent the aquation of 1 or 2 of the 2 chloride coordination sites in cisplatin, and only the aquated forms of cisplatin covalently bind to DNA. Nevertheless, the mechanisms of $[Cl^-]_i$ elevation because of cisplatin treatment have not been fully elucidated. We hypothesised that an increase in intracellular Ca^{2+} concentration after cisplatin exposure would result in translocation of ANXA4 from the cytosol to plasma membrane, which leads to $[Cl^-]_i$ accumulation through inhibition of the chloride channel by the Ca^{2+}-bound ANXA4. To confirm this hypothesis, we quantified $[Cl^-]_i$ after cisplatin treatment using MAQE fluorescence, a fluorescent Cl^- indicator. Relative fluorescence was substituted for $[Cl^-]_i$ as previously reported [48].

We monitored MQAE fluorescence in control cells (NC-14), in cells overexpressing full-length ANXA4 (FL-22) and in 2 deletion mutants (R1-12 and R1[E70A]-95). The relative fluorescence ratio before (F0) and after

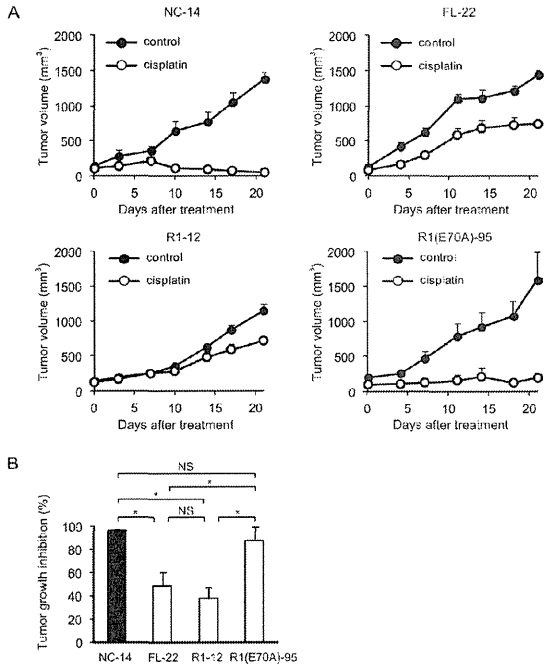

Fig.5: The calcium-binding site of the annexin repeat is required for platinum drug resistance *in vivo*. Female ICR *nu/nu* mice were subcutaneously inoculated with NC14, FL-22, R1-12 or R1(E70A)-95 cells and given PBS (control group: *filled circles*) or cisplatin i.p. (3 mg/kg; treatment group: *open circles*) once a week for 3 weeks (n = 6 per group). (A) Growth curves of tumours of each cell. The mean volume (points) ± SE (bars) is shown. (B) Comparison of the cisplatin-induced growth inhibition of tumours 28 days after treatment. The average (columns) ± SE (bars) are shown; *$p < 0.01$.

treatment with cisplatin for 30 min (F30) is shown in Figure 6. The inverse ratio of MQAE fluorescence 1/(F30/F0), which is directly proportional to the increase in $[Cl^-]_i$, was significantly elevated in the platinum-resistant cell clones FL-22 (1.12 ± 0.03) and R1-12 (1.12 ± 0.01) compared with sensitive clones, NC-14 (1.06 ± 0.01) and R1(E70A)-95 (1.06 ± 0.02; $p < 0.01$). Thus, the increase in $[Cl^-]_i$ is likely to be involved in cisplatin resistance.

DISCUSSION

ANXA4 has been reported to be strongly expressed and involved in chemoresistance in various cancers. The factors associated with ANXA4-induced chemoresistance have been reported, such as NF-κB [45] and ATP7A [44], but the structure of the protein, i.e. annexin repeats and calcium-binding sites in the annexin repeated sequence, has not been taken into account in relation to the ANXA4-induced chemoresistance. In this study, we showed that ANXA4 knockdown improved sensitivity to platinum drugs, and annexin repeats were involved in chemoresistance.

We first confirmed ANXA4 expression in various ovarian adenocarcinoma cell lines. As previously reported [28, 49], ANXA4 is significantly upregulated in clear cell carcinoma cell lines (OVTOKO, OVISE and RMG-I) compared with other histological types (serous and mucinous adenocarcinoma cell lines: A2780, OVCAR3, OVSAHO and MCAS). It has been previously demonstrated that enhanced ANXA4 expression induces platinum resistance both *in vitro* and *in vivo* [28, 44], but whether ANXA4 knockdown attenuates platinum resistance has been unknown thus far. Mogami et al. recently reported that an ANXA4 knockdown improves sensitivity to carboplatin *in vitro* using 2 cell lines of ovarian clear cell carcinoma, OVTOKO and OVISE. To the best of our knowledge, ours is the first study to show that ANXA4 knockdown markedly improves the sensitivity to platinum-based drugs not only *in vitro* but also *in vivo* (Figs. 1 and 2).

The result that ANXA4 knockdown improves sensitivity to platinum-based drugs suggests that ANXA4 is a good therapeutic target. To identify the functional domain(s) of ANXA4 that could be a promising therapeutic target, we focused on annexin repeats and constructed 4 deletion mutants (R3, R2, R1 and R1[E70A]). Resistance to platinum drugs was enhanced in cells transfected with mutants possessing at least 1 intact annexin repeat. In contrast, the sensitivity to platinum-based drugs improved among the R1(E70A)-transfected clones because in those cells, the calcium-binding site did not function properly (Figs. 3C and 4C). This result implies that the ANXA4-induced chemoresistance to platinum-based agents is calcium dependent. It has been reported that cisplatin induced increase of intracellular calcium concentration in chemosensitive cells, but not in resistant cells [46, 50]. Together with this and the data by Chan et al., elevation of intracellular calcium concentration induced by cisplatin treatment may translocate Ca^{2+} bound form of ANXA4 from cytosol to plasma membrane, which results in platinum-resistance[32]. We are currently investigating on further analysis.

By analysing the intracellular platinum accumulation, we attempted to elucidate the mechanism of the platinum resistance induced by ANXA4 and its deletion mutants. When intracellular platinum contents were quantitated just after exposure to cisplatin or 3 hr incubation with cisplatin-free medium after exposure to cisplatin, significantly less platinum accumulated in cells transfected with the full-length ANXA4 (FL-22) and 3 deletion mutants (R3-6, R2-13 and R1-12), all of which enhanced the resistance to the platinum-based drugs. In contrast, R1(E70A)-transfected cells (R1[E70A]-95), which did not induce chemoresistance, had the same amount of platinum accumulation as the control cells (Figs. 3D and 4D). These results suggest that the resistance to the platinum-based drugs is mediated by the decrease in intracellular platinum accumulation, which is calcium dependent. The annexin repeats, especially their calcium-binding sites, may be involved in inhibition of the influx, promotion of the efflux or both of platinum drugs. Recently, Cu transporters (CTR1 for the uptake and ATP7A and ATP7B for the efflux) have been reported to be involved in resistance to both cisplatin and carboplatin [14, 44, 51]. In addition, ANXA4 likely enhance platinum efflux through the interaction with ATP7A [44]. The possible mechanisms of inhibition of the influx mediated by ANXA4 remains unclear and further analyses are needed.

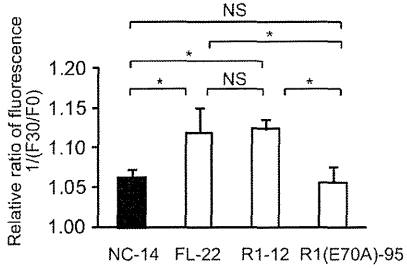

Fig.6: The increase of intracellular chloride concentration is related to cisplatin resistance. ANXA4 deletion mutant series cells (NC-14, FL-22, R1-12 and R1[E70A]-95) loaded with N-ethroxycarbonymethyl-6-methoxyquinolinium bromide (MQAE) were exposed to 100 μM cisplatin. The fluorescence pre-treatment and during treatment (30 min exposure) was compared in each cell clone. Data are presented as mean ± SD (*$p < 0.01$).

Subsequently, the question regarding the involvement of calcium-binding site in the platinum resistance arose. To answer this question, we measured $[Cl^-]_i$ after cisplatin exposure. The significant increase in $[Cl^-]_i$ was observed in the cells with platinum resistance, FL-22 and R1-12, compared with cell clones without platinum resistance, NC-14 and R1(E70A)-95. In a previous study, higher $[Cl^-]_i$ was observed in cisplatin-resistant cells compared with sensitive cells, whereas the intracellular cisplatin accumulation showed the opposite pattern [47]. These results, in addition to the results of decreased platinum accumulation in resistant mutants, indicate that ANXA4 induces platinum resistance through cellular drug efflux partly by elevating the intracellular chloride concentration. We report 'partly' because only cisplatin, not carboplatin, was tested in our $[Cl^-]_i$ assay. Cisplatin becomes intracellularly activated by the aquation of 1 or 2 of the 2 chloride coordination sites, but carboplatin does not contain any chloride coordination sites [1, 52-54]. Thus, this mechanism of resistance through elevation of $[Cl^-]_i$ may be specific to cisplatin and may not be true of carboplatin resistance. In this study, 3 cell clones overexpressing a deletion mutant (R3-6, R2-13, and R1-12) show stronger tolerance to cisplatin than to carboplatin in terms of their IC_{50}; a 1.7- to 2.2-fold increase for cisplatin and only a 1.4- to 1.7-fold increase for carboplatin (Fig. 3C). It is assumed that the increase in $[Cl^-]_i$ is one of the factors inducing cisplatin resistance.

In this study, the calcium-binding site in the annexin repeat next to the N terminus was observed to be responsible for the resistance to the platinum drugs. Nevertheless, the role of the other 3 calcium-binding sites has not yet been investigated. The roles of individual calcium-binding sites were demonstrated using site-directed mutagenesis by Nelson and Creutz regarding calcium-dependent membrane binding and aggregation [30]. The mutations in each domain had different effects on the binding or aggregating activities, i.e. a mutation in the first or fourth domain had a greater effect on membrane binding. A mutation in the second domain had a stronger effect on membrane aggregation, whereas the mutation of the third domain was almost silent. Although the mechanisms involved in membrane binding/aggregation and the mechanisms of chemoresistance are likely different, our data could provide some clues to understanding the function of each annexin repeat and each calcium-binding site in chemoresistance.

ANXA4 has been shown to induce resistance to paclitaxel and platinum-based drugs [55]. The effect of ANXA4 knockdown on paclitaxel sensitivity was assessed in a previous study. The effect of sensitivity to paclitaxel varied among different cell clones: ANXA4 knockdown in the OVTOKO cell line with acidic isoelectric point (IEPs) did not improve the sensitivity to paclitaxel, whereas OVISE cell lines with basic IEPs showed improved sensitivity to paclitaxel [43]. In our own preliminary data, significant chemosensitisation to paclitaxel and etoposide was confirmed in RMG-I Y4 and R5 (data not shown). Further studies are required to identify the detailed mechanism.

In summary, in this study, we observed the annexin repeat, especially its calcium binding site, was associated with platinum-resistance induced by ANXA4, and it happened in calcium-dependent manner. Our findings may help to understand the mechanisms of platinum resistance induced by other annexin family proteins, which possesses the same annexin repeat structure, and offer new strategies for the treatment of chemoresistant cancers.

METHODS

Cell lines and culture

The human ovarian serous adenocarcinoma cell line (OVSAHO), human ovarian mucinous adenocarcinoma cell line (MCAS), human ovarian clear cell carcinoma cell lines (OVTOKO, OVISE and RMG-I) and human gastric cancer cell line (NUGC3) were obtained from the Japanese Collection of Research Bioresources (Osaka, Japan). A2780 cells from the human ovarian serous adenocarcinoma were obtained from the European Collection of Animal Cell Culture (Salisbury, Scotland) and OVCAR-3 cells from another human ovarian serous adenocarcinoma were from American Type Culture Collection (Manassas, VA). MCAS cells were maintained in the DMEM medium and the others in the RPMI medium, all supplemented with 10% foetal bovine serum (FBS; Serum Source International, NC, USA) and 1% penicillin–streptomycin (Nacalai Tesque, Kyoto, Japan) at 37°C in a humidified atmosphere with 5% CO_2. All the cell lines were tested and authenticated.

Generation of ANXA4 knockdown cell lines

To generate stable ANXA4 knockdown cell lines, RMG-I cells were transfected with a commercial plasmid vector expressing short heparin RNA (shRNA) that targeted ANXA4 mRNA or a negative control nonspecific shRNA (SuperArray Bioscience Corp., KH06928N; Frederick, MD, USA) using Lipofectamine 2000 (Invitrogen, Carlsbad, CA), according to the manufacturer's instructions. After selection using a culture medium containing geneticin (600 μg/mL; Invitrogen), stable clones were maintained in 250 μg/mL geneticin. Two stable RMG-I-ANXA4 shRNA cell clones were established, designated Y4 and R5 cells. In addition, we transfected the empty vector into the RMG-I cell line using the same procedure to generate control cells, designated NC7.

Construction of ANXA4 deletion mutants and gene transfection

Using pcDNA3.1-ANXA4 as a template, full-length cDNA of ANXA4 was amplified using KOD-plus (Toyobo Co. Led., Osaka, Japan) with the primers forward 5′-TTGACCTAGAGTCATGGCCA-3′, reverse 5′-ATCATCTCCTCCACAGAGAA-3′ and subsequently ligated into the pcDNA3.1/V5-His-TOPO vector in-frame with the C-terminal V5 and 6× His tag. To generate ANXA4 deletion mutants, annexin repeat domains were deleted one by one from the C-terminal site. Three deletion mutants named R3, R2 and R1 were generated and similarly amplified (an Arabic number shows the number of annexin repeat domains). The nucleotide sequences of the forward primers for PCR were the same as those described above for all the deletion mutants, and the reverse primers were as follows: R3 5′-TATAGCCAGCAGAGCATCTT-3′, R2 5-CAGAGACACCAGCACTCGCT-3′ and R1 5′-CATCCCCACAATCACCTGCT-3′. We subsequently set out to generate an R1 mutant (the E70A mutation), whose calcium-binding site does not work because of the change of a negatively charged carboxyl group to a neutral side chain, as previously described [30]. The site-directed mutagenesis was performed using the KOD-Plus-Mutagenesis kit (Toyobo), according to the manufacturer's protocol. These cDNA fragments, including full-length gene, were subsequently inserted between the *Bgl* II and *EcoR* I sites of the pIRES2AcGFP vector (Clontech, Palo Alto, CA). The sequences of all the mutants were confirmed using the ABI PRISM 3100 Genetic Analyser (Applied Biosystems, Foster City, USA).

Full-length ANXA4, each ANXA4 deletion mutant construct and the empty vector were transfected into NUGC3 cells using Lipofectamine 2000 (Invitrogen). Stable transfectants designated FL-12, R3-6, R2-13, R1-12, R1(R70A)-95 and NC-14 were obtained by selection in a medium containing geneticin and were maintained in the same manner described above.

Western blotting

Cells were lysed in RIPA buffer (10 mM Tris–HCl, pH 7.5, 150 mM NaCl, 1% Nonidet P-40, 0.1% sodium deoxycholate, 0.1% SDS, 1× phosphatase inhibitor cocktail (Nacalai Tesque) and 1× protease inhibitor cocktail (Nacalai Tesque)), followed by centrifugation (13,200 rpm, 4°C, 15 min). Soluble proteins in the supernatant were separated using sodium dodecyl sulphate polyacrylamide gel electrophoresis, as described previously [28]. Additional information can be found in the Supporting Information on Material and Methods section.

Measurement of IC_{50} values after treatment with a platinum-based drug

Cells were suspended in the RPMI medium supplemented with 10% FBS, seeded in 96-well plates (1,500/well for the RMG-I series and 2,500 cells/well for ANXA4 deletion mutant series), cultured for 24 h and exposed to various concentrations of cisplatin (0–25 μM; Sigma–Aldrich, St Louis, MO) or carboplatin (0–1000 μM; Sigma–Aldrich) for 72 h. Cellular proliferation was subsequently evaluated using the WST-8 assay, i.e. 2-(2-methyosy-4-nitro-phenyl)-3-(4-nitrophenyl)-5-(2,4-disulfophynel)-2H-tetrazolium monosodium salt assay (Cell Counting Kit-SF; Nacalai Tesque) after treatment. The absorption of WST-8 was measured at a wavelength of 450 nm (reference wavelength: 630 nm) using a Model 680 microplate reader (Bio-Rad Laboratories, Hercules, CA). Absorbance values for the treated samples were expressed as percentages relative to results for untreated controls, and IC_{50} values were calculated.

Measurement of intracellular platinum accumulation

Full-length ANXA4-transfected cells (FL-22), each ANXA4 deletion mutant-transfected cell clone (R3-6, R2-13, R1-12 and R1[E70A]-95), and control cells (NC-14) were cultured up to 80% confluence in 150-mm tissue culture dishes. The cells were then exposed to 100 μM cisplatin for 60 min at 37°C and washed twice with PBS either immediately or after 3 hr of incubation in cisplatin-free RPMI 1640 medium supplemented with 10% FBS. Whole-cell extracts were prepared, and the concentration of intracellular platinum was determined using an Agilent 7500ce inductively coupled plasma mass spectrometer (ICP-MS; Agilent, Santa Clara, CA, USA).

In vivo model of cisplatin resistance

All animal experiments were conducted in accordance with the Institutional Ethical Guidelines for Animal Experimentation of the National Institute of Biomedical Innovation (Osaka, Japan). Female Institute of Cancer Research (ICR) *nu/nu* mice were obtained from Charles River Japan (Yokohama, Japan). Injection of the ANXA4 knockdown cells was performed as follows: ICR *nu/nu* mice at 4 weeks of age were subcutaneously inoculated (into the flank of the mice; n = 6 per group) with 2.5×10^6 cells of RMG-I NC7 cells or RMG-I-Y4 cells in the total volume of 100 μL of 1/1 (v/v) PBS/Matrigel (Becton Dickinson, Bedford, MA). Injection of ANXA4 mutant-transfected cells, i.e. mice at 5 weeks of age were inoculated with 10^6 cells of NC-14, FL-22, R1-12 or R1(E70A) in the same manner as with the ANXA4 knockdown cells. Treatment with cisplatin (3 mg/kg) or PBS *i.p.* was initiated 1 week after inoculation and administered twice weekly for 4 weeks (ANXA4 knockdown cells) and once a week for 3 weeks (ANXA4 mutant-transfected cells). Tumour volumes were determined twice weekly by measuring length (L), width (W) and depth (D) and using the following formula: tumour volume (mm^3) = W × L × D.

$[Cl^-]_i$ measurements

$[Cl^-]_i$ was measured using the fluorescent Cl^- indicator N-ethroxycarbonymethyl-6-methoxyquinolinium bromide (MQAE; Dojindo, Kumamoto, Japan). $[Cl^-]_i$ is detected by the mechanism of diffusion-limited collisional quenching of MQAE fluorescence. MQAE fluorescence intensity inversely correlates with $[Cl^-]_i$. The cells of the ANXA4 deletion mutant series (NC-14, FL-22, R1-12 and R1[E70A]-95) were cultured in 35-mm tissue culture dishes up to 20% confluence and incubated with a medium containing 10 mM MQAE for 4 h at 37°C. After loading, the cells were washed 5 times with Cl^--free buffer and electrically stimulated under a microscope at 37°C in a humidified atmosphere with 5% CO_2. Fluorescence measurements were initiated immediately at the indicated periods using Biozero BZ-9000 (Keyence, Tokyo, Japan) at 510/40 nm excitation and 380/50 nm emission. The fluorescence was quantitated by means of a standardised procedure using a BZ-II Analyser (Keyence), and the data were presented as the reciprocal of the ratio of fluorescence data (F0/F30) to identify possible correlations with the increase in $[Cl^-]_i$.

Statistical analysis

All calculations involved one-way analysis of variance (ANOVA) followed by Dunnett's analysis to evaluate the significance of differences. In all experiments, p value of <0.05 was considered statistically significant.

ACKNOWLEDGEMENTS

We thank Y. Kanazawa and A. Yagi for their secretarial assistance, M. Ako and E. Harada for technical assistance.

There are no conflicts of interest to declare. This study was supported by a Grant-in-Aid from the Program for Promotion of Fundamental Studies in Health Sciences of the National Institute of Biomedical Innovation; a Grant-in-Aid from the Ministry of Health, Labour and Welfare of Japan and Grants-in-Aid for Young Scientists (B) (22791560) from the Japanese Ministry of Education, Science, Culture and Sports

REFERENCES

1. Kelland L. The resurgence of platinum-based cancer chemotherapy. Nat Rev Cancer. 2007; 7(8):573-584.
2. Loriot Y, Mordant P, Deutsch E, Olaussen KA and Soria JC. Are RAS mutations predictive markers of resistance to standard chemotherapy? Nat Rev Clin Oncol. 2009; 6(9):528-534.
3. Alva AS, Matin SF, Lerner SP and Siefker-Radtke AO. Perioperative chemotherapy for upper tract urothelial cancer. Nat Rev Urol. 2012; 9(5):266-273.
4. Bookman MA. First-line chemotherapy in epithelial ovarian cancer. Clin Obstet Gynecol. 2012; 55(1):96-113.
5. Matos CS, de Carvalho AL, Lopes RP and Marques MP. New strategies against prostate cancer--Pt(II)-based chemotherapy. Curr Med Chem. 2012; 19(27):4678-4687.
6. Rossi A, Di Maio M, Chiodini P, Rudd RM, Okamoto H, Skarlos DV, Fruh M, Qian W, Tamura T, Samantas E, Shibata T, Perrone F, Gallo C, Gridelli C, Martelli O and Lee SM. Carboplatin- or cisplatin-based chemotherapy in first-line treatment of small-cell lung cancer: the COCIS meta-analysis of individual patient data. J Clin Oncol. 2012; 30(14):1692-1698.
7. Muggia FM and Los G. Platinum resistance: laboratory findings and clinical implications. Stem Cells. 1993; 11(3):182-193.
8. Jassem J. Chemotherapy of advanced non-small cell lung cancer. Ann Oncol. 1999; 10 Suppl 6:77-82.
9. Perez RP. Cellular and molecular determinants of cisplatin resistance. Eur J Cancer. 1998; 34(10):1535-1542.
10. Fuertes MA, Castilla J, Alonso C and Perez JM. Novel concepts in the development of platinum antitumor drugs. Curr Med Chem Anticancer Agents. 2002; 2(4):539-551.
11. Gonzalez VM, Fuertes MA, Alonso C and Perez JM. Is cisplatin-induced cell death always produced by apoptosis? Mol Pharmacol. 2001; 59(4):657-663.
12. Niedner H, Christen R, Lin X, Kondo A and Howell SB. Identification of genes that mediate sensitivity to cisplatin. Mol Pharmacol. 2001; 60(6):1153-1160.
13. Ishida S, Lee J, Thiele DJ and Herskowitz I. Uptake of the anticancer drug cisplatin mediated by the copper transporter Ctr1 in yeast and mammals. Proc Natl Acad Sci U S A. 2002; 99(22):14298-14302.
14. Safaei R, Holzer AK, Katano K, Samimi G and Howell SB. The role of copper transporters in the development of resistance to Pt drugs. J Inorg Biochem. 2004; 98(10):1607-1613.
15. Katano K, Kondo A, Safaei R, Holzer A, Samimi G, Mishima M, Kuo YM, Rochdi M and Howell SB. Acquisition of resistance to cisplatin is accompanied by changes in the cellular pharmacology of copper. Cancer Res. 2002; 62(22):6559-6565.
16. Samimi G, Varki NM, Wilczynski S, Safaei R, Alberts DS and Howell SB. Increase in expression of the copper

transporter ATP7A during platinum drug-based treatment is associated with poor survival in ovarian cancer patients. Clin Cancer Res. 2003; 9(16 Pt 1):5853-5859.

17. Rabik CA, Maryon EB, Kasza K, Shafer JT, Bartnik CM and Dolan ME. Role of copper transporters in resistance to platinating agents. Cancer Chemother Pharmacol. 2009; 64(1):133-142.
18. Koike K, Kawabe T, Tanaka T, Toh S, Uchiumi T, Wada M, Akiyama S, Ono M and Kuwano M. A canalicular multispecific organic anion transporter (cMOAT) antisense cDNA enhances drug sensitivity in human hepatic cancer cells. Cancer Res. 1997; 57(24):5475-5479.
19. Cui Y, Konig J, Buchholz JK, Spring H, Leier I and Keppler D. Drug resistance and ATP-dependent conjugate transport mediated by the apical multidrug resistance protein, MRP2, permanently expressed in human and canine cells. Mol Pharmacol. 1999; 55(5):929-937.
20. Liedert B, Materna V, Schadendorf D, Thomale J and Lage H. Overexpression of cMOAT (MRP2/ABCC2) is associated with decreased formation of platinum-DNA adducts and decreased G2-arrest in melanoma cells resistant to cisplatin. J Invest Dermatol. 2003; 121(1):172-176.
21. Ban N, Takahashi Y, Takayama T, Kura T, Katahira T, Sakamaki S and Niitsu Y. Transfection of glutathione S-transferase (GST)-pi antisense complementary DNA increases the sensitivity of a colon cancer cell line to adriamycin, cisplatin, melphalan, and etoposide. Cancer Res. 1996; 56(15):3577-3582.
22. Olaussen KA, Dunant A, Fouret P, Brambilla E, Andre F, Haddad V, Taranchon E, Filipits M, Pirker R, Popper HH, Stahel R, Sabatier L, Pignon JP, Tursz T, Le Chevalier T and Soria JC. DNA repair by ERCC1 in non-small-cell lung cancer and cisplatin-based adjuvant chemotherapy. N Engl J Med. 2006; 355(10):983-991.
23. Wang Q, Shi S, He W, Padilla MT, Zhang L, Wang X, Zhang B and Lin Y. Retaining MKP1 expression and attenuating JNK-mediated apoptosis by RIP1 for cisplatin resistance through miR-940 inhibition. Oncotarget. 2014; 5(5):1304-1314.
24. Li H and Yang BB. MicroRNA in drug resistance. Oncoscience. 2014; 1(1):2.
25. Yang H, Kong W, He L, Zhao JJ, O'Donnell JD, Wang J, Wenham RM, Coppola D, Kruk PA, Nicosia SV and Cheng JQ. MicroRNA expression profiling in human ovarian cancer: miR-214 induces cell survival and cisplatin resistance by targeting PTEN. Cancer Res. 2008; 68(2):425-433.
26. Sorrentino A, Liu CG, Addario A, Peschle C, Scambia G and Ferlini C. Role of microRNAs in drug-resistant ovarian cancer cells. Gynecol Oncol. 2008; 111(3):478-486.
27. Perego P, Giarola M, Righetti SC, Supino R, Caserini C, Delia D, Pierotti MA, Miyashita T, Reed JC and Zunino F. Association between cisplatin resistance and mutation of p53 gene and reduced bax expression in ovarian carcinoma cell systems. Cancer Res. 1996; 56(3):556-562.
28. Kim A, Enomoto T, Serada S, Ueda Y, Takahashi T, Ripley B, Miyatake T, Fujita M, Lee CM, Morimoto K, Fujimoto M, Kimura T and Naka T. Enhanced expression of Annexin A4 in clear cell carcinoma of the ovary and its association with chemoresistance to carboplatin. Int J Cancer. 2009; 125(10):2316-2322.
29. Gerke V and Moss SE. Annexins: from structure to function. Physiol Rev. 2002; 82(2):331-371.
30. Nelson MR and Creutz CE. Combinatorial mutagenesis of the four domains of annexin IV: effects on chromaffin granule binding and aggregating activities. Biochemistry. 1995; 34(9):3121-3132.
31. Kaetzel MA, Hazarika P and Dedman JR. Differential tissue expression of three 35-kDa annexin calcium-dependent phospholipid-binding proteins. J Biol Chem. 1989; 264(24):14463-14470.
32. Chan HC, Kaetzel MA, Gotter AL, Dedman JR and Nelson DJ. Annexin IV inhibits calmodulin-dependent protein kinase II-activated chloride conductance. A novel mechanism for ion channel regulation. J Biol Chem. 1994; 269(51):32464-32468.
33. Kaetzel MA, Mo YD, Mealy TR, Campos B, Bergsma-Schutter W, Brisson A, Dedman JR and Seaton BA. Phosphorylation mutants elucidate the mechanism of annexin IV-mediated membrane aggregation. Biochemistry. 2001; 40(13):4192-4199.
34. Dreier R, Schmid KW, Gerke V and Riehemann K. Differential expression of annexins I, II and IV in human tissues: an immunohistochemical study. Histochem Cell Biol. 1998; 110(2):137-148.
35. Wei R, Zhang Y, Shen L, Jiang W, Li C, Zhong M, Xie Y, Yang D, He L and Zhou Q. Comparative proteomic and radiobiological analyses in human lung adenocarcinoma cells. Mol Cell Biochem. 2012; 359(1-2):151-159.
36. Alfonso P, Canamero M, Fernandez-Carbonie F, Nunez A and Casal JI. Proteome analysis of membrane fractions in colorectal carcinomas by using 2D-DIGE saturation labeling. J Proteome Res. 2008; 7(10):4247-4255.
37. Zimmermann U, Balabanov S, Giebel J, Teller S, Junker H, Schmoll D, Protzel C, Scharf C, Kleist B and Walther R. Increased expression and altered location of annexin IV in renal clear cell carcinoma: a possible role in tumour dissemination. Cancer Lett. 2004; 209(1):111-118.
38. Sitek B, Luttges J, Marcus K, Kloppel G, Schmiegel W, Meyer HE, Hahn SA and Stuhler K. Application of fluorescence difference gel electrophoresis saturation labelling for the analysis of microdissected precursor lesions of pancreatic ductal adenocarcinoma. Proteomics. 2005; 5(10):2665-2679.
39. Xin W, Rhodes DR, Ingold C, Chinnaiyan AM and Rubin MA. Dysregulation of the annexin family protein family is associated with prostate cancer progression. Am J Pathol. 2003; 162(1):255-261.
40. Duncan R, Carpenter B, Main LC, Telfer C and Murray GI. Characterisation and protein expression profiling of annexins in colorectal cancer. Br J Cancer. 2008; 98(2):426-433.
41. Yamashita T, Nagano K, Kanasaki S, Maeda Y, Furuya T, Inoue M, Nabeshi H, Yoshikawa T, Yoshioka Y, Itoh N, Abe Y, Kamada H, Tsutsumi Y and Tsunoda S. Annexin A4 is a possible biomarker for cisplatin susceptibility of malignant mesothelioma cells. Biochem Biophys Res Commun. 2012; 421(1):140-144.
42. Choi CH, Sung CO, Kim HJ, Lee YY, Song SY, Song T, Kim J, Kim TJ, Lee JW, Bae DS and Kim BG. Overexpression of annexin A4 is associated with chemoresistance in papillary serous adenocarcinoma of the ovary. Hum Pathol. 2013; 44(6):1017-1023.
43. Mogami T, Yokota N, Asai-Sato M, Yamada R, Koizume S, Sakuma Y, Yoshihara M, Nakamura Y, Takano Y, Hirahara F, Miyagi Y and Miyagi E. Annexin a4 is involved in proliferation, chemo-resistance and migration and invasion in ovarian clear cell adenocarcinoma cells. PLoS One. 2013; 8(11):e80359.
44. Matsuzaki S, Enomoto T, Serada S, Yoshino K, Nagamori S, Morimoto A, Yokoyama T, Kim A, Kimura T, Ueda Y, Fujita M, Fujimoto M, Kanai Y and Naka T. Annexin A4-conferred platinum resistance is mediated by the copper transporter ATP7A. Int J Cancer. 2013.
45. Jeon YJ, Kim DH, Jung H, Chung SJ, Chi SW, Cho S, Lee SC, Park BC, Park SG and Bae KH. Annexin A4 interacts with the NF-kappaB p50 subunit and modulates NF-kappaB transcriptional activity in a Ca2+-dependent manner. Cell Mol Life Sci. 2010; 67(13):2271-2281.
46. Al-Bahlani S, Fraser M, Wong AY, Sayan BS, Bergeron R, Melino G and Tsang BK. P73 regulates cisplatin-induced apoptosis in ovarian cancer cells via a calcium/calpain-dependent mechanism. Oncogene. 2011; 30(41):4219-4230.
47. Salerno M, Yahia D, Dzamitika S, de Vries E, Pereira-Maia E and Garnier-Suillerot A. Impact of intracellular chloride concentration on cisplatin accumulation in sensitive and resistant GLC4 cells. J Biol Inorg Chem. 2009; 14(1):123-132.
48. Chao AC, Dix JA, Sellers MC and Verkman AS. Fluorescence measurement of chloride transport in monolayer cultured cells. Mechanisms of chloride transport in fibroblasts. Biophys J. 1989; 56(6):1071-1081.
49. Masuishi Y, Arakawa N, Kawasaki H, Miyagi E, Hirahara F and Hirano H. Wild-type p53 enhances annexin IV gene expression in ovarian clear cell adenocarcinoma. FEBS J. 2011; 278(9):1470-1483.
50. Splettstoesser F, Florea AM and Busselberg D. IP(3) receptor antagonist, 2-APB, attenuates cisplatin induced Ca2+-influx in HeLa-S3 cells and prevents activation of calpain and induction of apoptosis. Br J Pharmacol. 2007; 151(8):1176-1186.
51. Safaei R. Role of copper transporters in the uptake and efflux of platinum containing drugs. Cancer Lett. 2006; 234(1):34-39.
52. El-Khateeb M, Appleton TG, Charles BG and Gahan LR. Development of HPLC conditions for valid determination of hydrolysis products of cisplatin. J Pharm Sci. 1999; 88(3):319-326.
53. Kelland LR. Preclinical perspectives on platinum resistance. Drugs. 2000; 59 Suppl 4:1-8; discussion 37-38.
54. Siddik ZH. Cisplatin: mode of cytotoxic action and molecular basis of resistance. Oncogene. 2003; 22(47):7265-7279.
55. Gaudio E, Paduano F, Spizzo R, Ngankeu A, Zanesi N, Gaspari M, Ortuso F, Lovat F, Rock J, Hill GA, Kaou M, Cuda G, Aqeilan RI, Alcaro S, Croce CM and Trapasso F. Fhit delocalizes annexin a4 from plasma membrane to cytosol and sensitizes lung cancer cells to Paclitaxel. PLoS One. 2013; 8(11):e78610

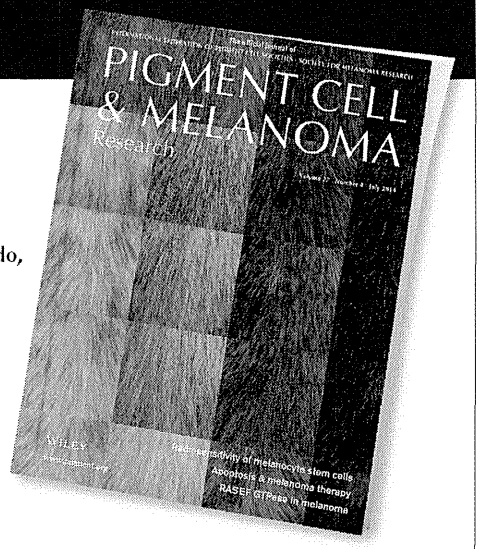

Periostin accelerates human malignant melanoma progression by modifying the melanoma microenvironment

Yorihisa Kotobuki[1,2,a], Lingli Yang[1,a], Satoshi Serada[2], Atsushi Tanemura[1], Fei Yang[1], Shintaro Nomura[3], Akira Kudo[4], Kenji Izuhara[5], Hiroyuki Murota[1], Minoru Fujimoto[2], Ichiro Katayama[1] and Tetsuji Naka[2]

1 Department of Dermatology, Osaka University Graduate School of Medicine, Suita, Japan **2** Laboratory for Immune Signal, National Institute of Biomedical Innovation, Ibaraki, Japan **3** Department of Animal Bioscience, Nagahama Institute of Bio-Science and Technology, Nagahama, Japan **4** Department of Biological Information, Tokyo Institute of Technology, Yokohama, Japan **5** Division of Medical Biochemistry, Department of Biomolecular Sciences, Saga Medical School, Saga, Japan

CORRESPONDENCE Atsushi Tanemura, e-mail: tanemura@derma.med.osaka-u.ac.jp

[a]These two authors contributed equally to this work.

KEYWORDS periostin/malignant melanoma/tumor microenvironment

PUBLICATION DATA Received 29 May 2013, revised and accepted for publication 24 March 2014, published online 26 March 2014

doi: 10.1111/pcmr.12245

Summary

Given no reliable therapy for advanced malignant melanoma, it is important to elucidate the molecular mechanisms underlying the disease progression. Using a quantitative proteomics approach, the 'isobaric tags for relative and absolute quantitation (iTRAQ)' method, we identified that the extracellular matrix protein, periostin (POSTN), was highly expressed in invasive melanoma compared with normal skin. An immunohistochemical analysis showed that POSTN was expressed in all invasive melanoma (n = 20) and metastatic lymph node (n = 5) tissue samples, notably restricted in their stroma. In terms of the intercellular regulation of POSTN, we found that there was upregulation of POSTN when melanoma cells and normal human dermal fibroblasts (NHDFs) were cocultured, with restricted expression of TGF-β1 and TGF-β3. In a functional analyses, recombinant and NHDF-derived POSTN significantly accelerated melanoma cell proliferation via the integrin/mitogen-activated protein kinase (MAPK) signaling pathway in vitro. The size of implanted melanoma tumors was significantly suppressed in *POSTN/Rag2* double knockout mice compared with *Rag2* knock-out mice. These results indicate that NHDF-derived POSTN accelerates melanoma progression and might be a promising therapeutic target for malignant melanoma.

Significance

In this study, we found an extracellular matrix protein, periostin (POSTN), increased in invasive melanoma compared with radial growth melanoma a quantitative proteomics approach, the 'isobaric tags for relative and absolute quantitation (iTRAQ)' method. POSTN was exclusively expressed in the tumor-associated stromal tissue not in the tumor cells, suggesting the paracrine effect of POSTN to melanoma cells aggressiveness. As expected, secreted POSTN could augment cell proliferation in melanoma cell lines in vitro. Moreover, we generated of *postn* and *rag2* double knockout mice and showed significant inhibition of human melanoma growth in those *KO* mice in vivo. This study could give us the cue of therapeutic effect on melanoma growth by an agent controlling tumor microenvironment induced by POSTN.

Introduction

Malignant melanoma is one of the most aggressive malignancies due to its strong capacity to grow, invade and metastasize, and therefore, it is of high priority to identify novel therapeutic targets and treatment options for this cancer.

Periostin (POSTN), first described in 1993 in mouse osteoblasts as osteoblast-specific factor 2 (OSF-2), is a secreted matrix N-glycoprotein of 93 kDa (Takeshita et al., 1993). The N-terminal region contains four fasciclin-like domains as well as several glycosylation sites. The protein originally was identified in MC3T3-E1 osteoblast-like cells, where it promotes integrin-dependent cell adhesion and motility. It shares homology with the insect cell adhesion molecule fasciclin I, with human β IgH3, and is induced by transforming growth factor-β (TGF-β) (Horiuchi et al., 1999), bone morphogenic protein-2 (Inai et al., 2008), IL-4, IL-13 (Takayama et al., 2006), and PDGF-bb (Li et al., 2006). As a ligand to alpha(V)beta(3) and alpha(V)beta(5) integrins, POSTN appears to activate the Akt/PKB (protein kinase B) pathway, which is known to facilitate cell survival and tumorigenesis (Bao et al., 2004; Gillan et al., 2002; Yan and Shao, 2006).

POSTN promotes the epithelial–mesenchymal transition (EMT), cancer cell growth, angiogenesis, invasiveness, and metastasis in several cancers (Bao et al., 2004; Baril et al., 2007; Erkan et al., 2007; Gillan et al., 2002; Kudo et al., 2006; Li et al., 2002; Puppin et al., 2008; Riener et al., 2010; Sasaki et al., 2001, 2002, 2003; Shao et al., 2004; Soltermann et al., 2008a,b; Tilman et al., 2007; Tischler et al., 2010). Although it was also reported that melanomas expressed POSTN (Tilman et al., 2007), the precise roles and the source of POSTN in malignant melanoma are still unclear.

We investigated the functional role of POSTN during melanoma tumor progression in vitro *and* in vivo. Moreover, we herein demonstrate that stromal cells, normal human dermal fibroblasts (NHDFs), were important sources of POSTN in cutaneous malignant melanoma and that NHDFs promote tumor growth and progression and modulate the tumor microenvironment by secreting POSTN in cutaneous malignant melanoma.

Results

Protein expression profiles in melanoma and normal skin

To identify the proteins associated with the progression of melanoma, we performed comparative protein expression profiling between in situ melanoma tissues and matched normal skin tissue, or between invasive melanoma tissue and matched normal skin tissues. We identified a total of 1062 proteins, and 1036 proteins were quantitatively analyzed by the iTRAQ 4-plex technology using a nano LC-MS/MS analysis. The complete list of all proteins identified is shown in Table S1. Among the identified proteins present at different levels in the invasive melanoma lesions compared with matched normal skin, 30 proteins were found to have increased more than 15-fold, while 67 proteins decreased to <0.25-fold (Table S1). As expected, S100, a protein previously known to be overexpressed in melanoma, was identified as one of the overexpressed proteins. Interestingly, POSTN was found to have a 25.703-fold higher expression in invasive tumor tissue compared with matched normal skin and showed a 4.434-fold higher expression in in situ tissue compared with matched normal skin (Table S1).

Expression of POSTN in melanomas

To confirm the altered expression of POSTN in invasive melanoma, we performed a Western blot analysis using proteins extracted from the same samples. As shown in Figure 1, POSTN was highly expressed in invasive melanoma tissue and slightly expressed in in situ tissue, although POSTN was faint in normal skin tissue (Figure 1A).

We thereafter preformed an immunohistochemical analysis of 20 invasive melanoma tissues and five metastatic lymph nodes. The expression of POSTN was observed in all invasive melanoma tissue samples and metastatic lymph nodes (Figure 1B). POSTN was localized in the stroma of the invasive melanoma, with a mesh-like structure (Figure 1C). Together, these data demonstrate that POSTN was overexpressed in invasive melanoma at the protein level; this was consistent with the results of our iTRAQ analysis.

POSTN is produced by NHDF instead of melanoma cells

We also analyzed the expression of POSTN in the cell lysates from three melanoma cell lines (MeWo, G-361, and VMRC-MELG) and melanocytes by Western blot analysis; however, the expression of POSTN was not observed in these cells (Figure 2A). Because POSTN was expressed in melanoma tissue samples, but not in melanoma cell lines, we hypothesized that an interaction between melanoma cells and NHDFs was required for the optimum expression of POSTN. First, we cocultured NHDFs with the MeWo, G-361, and VMRC-MELG cell lines and performed RT-PCR and a Western blot analysis. An overexpression of POSTN mRNA was only observed in the cocultured cell lysates (Figure 2B), and POSTN protein was detected in the cocultured supernatant in a time-dependent manner (Figure 2C).

To identify the source of POSTN, we cocultured NHDFs with CFSE-labeled MeWo cells for 48 h, and sorted these cells into NHDF and MeWo populations. The expression of POSTN mRNA measured by RT-PCR showed the source of the POSTN to be the NHDFs, not the MeWo cells (Figure 2D).

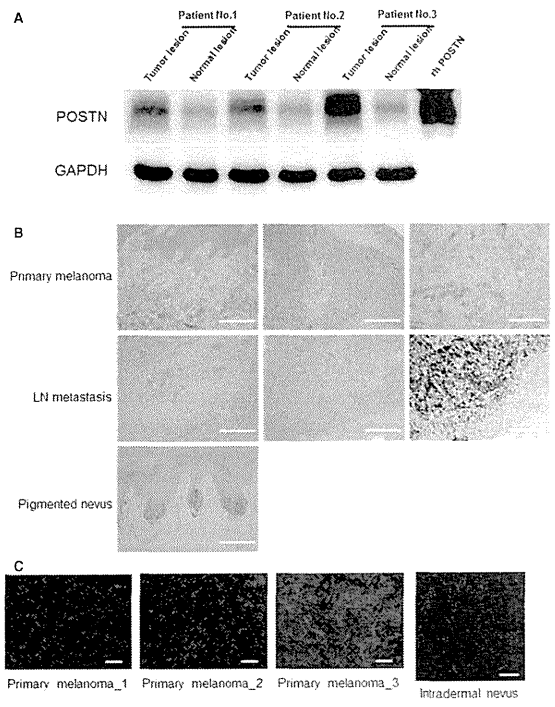

Figure 1. POSTN expression is much higher in melanoma tumor tissues compared with normal lesions. POSTN is predominantly expressed in the stroma of the melanoma tumors not melanoma cells. POSTN was slightly expressed in the in situ melanoma tissues (patient No. 1, No. 2) and highly expressed in the invasive melanoma tissues (patient No. 3) in a Western blot analysis (A). POSTN staining of invasive melanoma samples (upper three panels) and metastatic lymph nodes (middle three panels), but no expression of POSTN was detected in the pigmented nevus (lower left panel). Positive cells are stained red with ALP colorization. Bar indicates 100 μm (B). The confocal microscopic analysis showed that POSTN was strongly expressed in the stromal tissue with a lattice pattern in the 3 melanoma tissues (left 3 panels) not in the intradermal nevus (right panel). Bar indicates 20 μm for melanoma and 10 μm for intradermal nevus, respectively (C).

TGF-β1 and TGF-β3 mRNA expression in NHDFs after the coculture with melanoma cells

While the coculture of NHDF and melanoma cells was effective for the induction of POSTN expression, it was unclear how POSTN was induced during the coculture. To *investigate the effect of soluble factors secreted by* melanoma cells, we cultured NHDFs in the conditioned medium from MeWo or G-361 cells, and measured the expression of POSTN. However, the overexpression of POSTN was not observed at the protein level during these experiments (Figure 2E).

Next, to detect the soluble factors inducing POSTN in NHDFs, we *examined the expression of POSTN-inducing* cytokines, such as TGF-β1, 3, IL-4, IL-13, BMP2, and PDGF-bb, which are known to be soluble inducers of POSTN. During the RT-PCR analysis, IL-4, IL-13, BMP2, and PDGF-bb mRNA were not affected after the cocultured of melanoma cells and NHDFs (Figure 2F). However, TGF-β1 and TGF-β3 mRNA were both significantly upregulated in the cocultured NHDFs (Figure 2F). In addition, neutralization of TGF-β in the coculture markedly blocked the increase in POSTN expression (Figure 2G).

These findings indicate that cell–cell contact between NHDFs and melanoma cells is important for the expression of TGF-βs and POSTN from NHDFs, but the secretion of proteins from melanoma cells is not important for this effect.

Expression of integrin $\alpha v\beta 3$ and $\alpha v\beta 5$ in melanoma cells

Because integrin $\alpha v\beta 3$, $\alpha v\beta 5$, and $\alpha 6\beta 4$ are well-known receptors for POSTN, we investigated the expression of these molecules by a Western blot analysis. We observed the expression of integrin $\alpha v\beta 3$ and $\alpha v\beta 5$ in the MeWo and G-361 cell lines (Figure 3A). On the other hand, integrin $\alpha 6\beta 4$ was not expressed in the melanoma cells (data not shown).

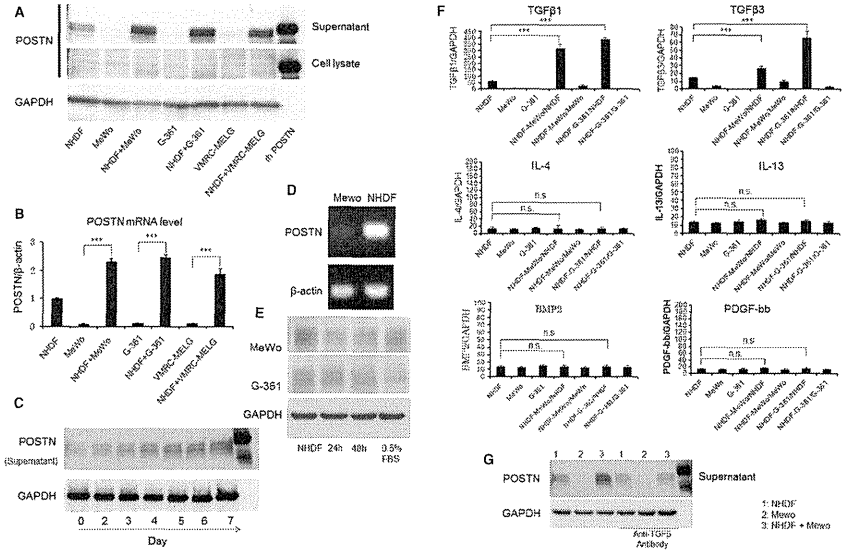

Figure 2. NHDFs secret POSTN during the coculture with human melanoma cells. The POSTN protein was upregulated in the supernatant after the coculture of NHDFs with human melanoma cells as determined by a Western blot analysis (A). POSTN mRNA was upregulated in the cell lysates after the coculture of NHDFs with human melanoma cells (B). POSTN expression was upregulated in the coculture media in a time-dependent manner (C). NHDFs, but not MeWo cells, induced POSTN expression under the coculture conditions (D). POSTN was not upregulated in the treatment with the conditioned media (E). The levels of TGFβ1, TGFβ3, IL-4, IL-13, BMP2, and PDGF-bb from NHDFs were increased after the coculture of NHDFs with melanoma cells (F). POSTN expressions were evaluated in cultured cells with or without anti-TGF-β neutralizing antibody (10 μg/ml, #MAB1835, R&D system, Minneapolis, MN). Neutralization of TGF-β blocked the increase in POSTN periostin in cocultured NHDF (G). *** indicate P-value <0.001.

Recombinant POSTN protein accelerates the proliferation of melanoma cells

To investigate the role of POSTN in the proliferation of human melanoma, we performed the MTT proliferation assay using recombinant human POSTN. The melanoma cells proliferated significantly more than control cells following the treatment with recombinant POSTN (Figure 3B). The proliferation in response to the treatment with recombinant POSTN was suppressed by anti-integrin $\alpha v\beta 3$ and $\alpha v\beta 5$ antibodies, which can neutralize the stimulation by POSTN (Figure 3C).

The phosphorylation of Akt and p44/42MAPK was observed in the cells treated with 100 ng/ml of recombinant POSTN (Figure 3D). However, the proliferation in response to the treatment with recombinant POSTN was abrogated by treatment with a MAPK inhibitor (PD98095), but not with an Akt inhibitor (LY294002) (Figure 3E). These results indicate that POSTN promotes melanoma proliferation *via* the integrin/p44/42MAPK pathway.

NHDF-derived POSTN gene transfection promotes the proliferation of melanoma cells

To investigate the role of NHDF-derived POSTN in melanoma, we transfected the NHDF-derived POSTN gene into MeWo cells (POSTN-low: lower POSTN expressing MeWo cells, POST-high: higher POSTN expressing MeWo cells, Figure 4A) and performed the MTT proliferation assay. The proliferation of POSTN–MeWo cells was significantly upregulated compared with control–MeWo (CTL-MeWo) cells in a time-dependent manner and much higher in POSTN-high cells (Figure 4B).

Significant suppression of human melanoma tumor growth in *POSTN* gene-deficient mice

We established immunodeficient Rag2 knockout mice (*Rag2* KO mice) and POSTN and Rag2 double knockout mice (*POSTN/Rag2* KO mice). We transplanted the MeWo human melanoma cell line subcutaneously onto the back of each of 17 mice and measured the tumor size for 70 days. The resulting tumors were smaller in the

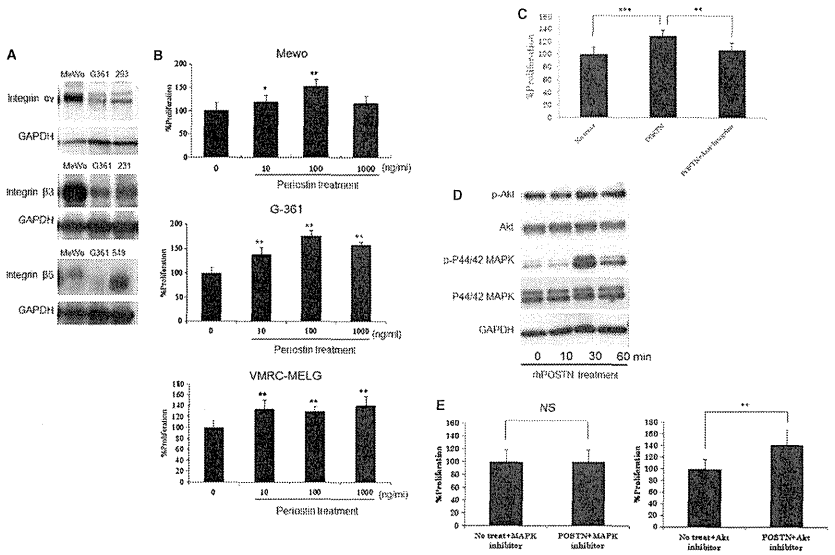

Figure 3. Recombinant POSTN protein accelerates melanoma cell proliferation via the integrin/P44/42MAPK pathway. Integrins αv, β3, and β5 were expressed in human melanoma cell lines (A). Recombinant POSTN increased the proliferation of human melanoma cells (MeWo, G-361, VMRC-MELG) (B). Neutralization of integrins $\alpha v\beta 3$ and $\alpha v\beta 5$ inhibited MeWo proliferation after the treatment with recombinant POSTN (C). The phosphorylation of Akt and P44/42MAPK in MeWo cells after the indicated treatment (D). Significant inhibition of MeWo cell proliferation after the treatment with recombinant POSTN by MAPK or Akt inhibitor (E). *, **, and *** indicate P-value <0.05, <0.01, <0.001, respectively.

double KO mice on day 56 after transplantation compared with the single KO mice (Figure 5A). The number of Ki-67-positive cells was significantly lower in the double KO mice compared with *Rag2* KO mice which indicated decrease in cell proliferation (Figure 5B, C). The levels of the αSMA protein, known as a marker of myofibroblasts and collagen tissue, which is colored red with E-V (Elastica van Gieson) staining, were decreased (Figure 5B). The growth of implanted melanoma tumors was also significantly suppressed in the double KO mice (Figure 5D).

Discussion

In this study, we reported the expression and function of POSTN in the ontogeny and progression of human malignant melanoma. We first noted the upregulation of POSTN protein expression in melanoma tissues compared with adjacent normal skin using an iTRAQ analysis, thereafter confirmed that higher expression in invasive melanoma. These results suggested that the upregulation of POSTN expression might be associated with the tumor malignancy. In the confocal microscopic analysis, POSTN was predominantly found to be distinctively localized in the stroma of invasive melanoma tissue, but not in cultured melanoma cells, thus suggesting the possibility that POSTN is derived from NHDFs to affect the melanoma microenvironment. The coculture of human melanoma cells with NHDFs robustly induced POSTN expression. These results indicate that POSTN expression is produced by NHDFs, but not by melanoma cells.

Recent studies have revealed that interactions between tumor cells and the surrounding stroma play an important role in facilitating tumor growth and invasion. In the present study, the induction of TGF-β in NHDF was found by melanoma cell–NHDF cell contact, and the behavior of dermal fibroblasts was altered to promote tumor growth and invasion by the interaction with surrounding melanoma cells. As reported previously, integrin was found to activate autocrine TGF-β signaling (Asano Y et al., 2005). In the present study, integrin was found highly expressed in melanoma cells (Figure 3). It suggested the similar mechanism of activated autocrine TGF-β signaling by integrin might be involved in the interaction of melanoma cell–NHDF.

Recent studies have revealed the importance of the fibrotic microenvironments surrounding cancer cells and the interactions between the host tissue and cancer cells

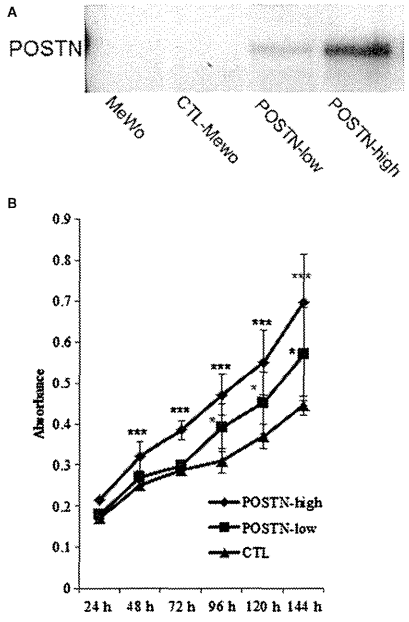

Figure 4. There is a significant increase in the proliferation of *POSTN*-transfected MeWo cells. *POSTN* gene transfection into MeWo cells (A). *POSTN* gene transfection upregulates the proliferation of MeWo cells (B). * and *** indicate P-value <0.05, <0.001, respectively.

for tumor growth and progression, because tumors are dependent on the normal host tissue-derived stromal cells and vasculature for growth and sustenance (Hanahan and Weinberg, 2000; Nyberg et al., 2008; Polyak and Kalluri, 2010; Quaranta, 2002; Yang et al., 2003; Zeisberg et al., 2002). Although there has been no previous report of a role of POSTN as stromal microenvironment in malignant melanoma, our data suggest that such a role exists.

We previously reported that POSTN accelerates dermal fibroblast proliferation, migration (Ontsuka et al., 2012), and myofibroblast differentiation, collagen 1 production (Yang et al., 2012), resulting in dermal fibrosis, and Elliott et al. also revealed the modulation of myofibroblast differentiation by POSTN (Elliott et al., 2012). These data support that NHDF-derived POSTN overexpression in the stroma of melanoma could affect the stromal microenvironment by activating dermal fibroblasts followed by tumor progression. In another report, impaired fibrous capsule formation of the implanted tumor was found in *periostin*-null mice, resulting in accelerating the tumor expansion (Guarino, 2010). Although our present data seem to be opposite of the previous report, MeWo cell established from human melanoma did not histologically form the surrounding fibrous capsule and the tumor immunity was canceled on the basis of Rag2 KO immune-deficient mice. Periostin expressed on intertumor space may be affected to accelerate adjacent melanoma cells in the present study setting.

We also revealed the proliferative effect of POSTN in human melanoma using recombinant and NHDF-derived POSTN. In details, we investigated the phosphorylation of FAK, STAT3, Akt, and p44/42MAPK, which are known to be the downstream pathways of integrin signals (Guarino, 2010). We did not observe any increase in the phosphorylation of FAK or STAT3 (data not shown), but upregulated phosphorylation of Akt and p44/42MAPK was observed after the treatment with recombinant POSTN. We also revealed that the proliferative effect of POSTN in melanoma is mediated by the integrins $\alpha v\beta 3$ and $\alpha v\beta 5$/p44/42MAPK signaling pathway, but not by the Akt pathway which is previously reported pathway (Bao et al., 2004; Ouyang et al., 2009; Yang et al., 2012).

To investigate the agonistic effect of POSTN on melanoma tissue growth in vivo, we transplanted MeWo cells into Rag2 KO mice and POSTN/Rag2 KO mice. The number of cells that were positive for Ki-67 was significantly decreased in the tumors of POSTN KO mice. In addition, the number of αSMA positive cells and the collagen expression which are known to be induced by POSTN in our previous study (Yang et al., 2012) were also decreased in POSTN KO melanomas, thus suggesting that there was suppression of the stromal microenvironment in these melanomas.

It has been reported that the POSTN expression in several cancers plays important roles in cancer progression as a result of increased proliferation, migration (Gillan et al., 2002), EMT (Soltermann et al., 2008a,b), and angiogenesis (Shao et al., 2004). In this study, our findings showed the source of POSTN to be restricted to NHDFs in human melanoma tissues, and that these stromal NHDFs between tumor cells may activate melanoma cell progression and invasion through an enhanced deposition of POSTN in the melanoma microenvironment.

Recent advances in the therapeutic approach for advanced melanoma have led to many clinical trials for patients with melanoma. For example, a BRAF inhibitor was reported to dramatically improve the prognosis of patients with melanoma. However, it was only effective in patients with the *V600E* gene mutation in the tyrosine kinase site (Atefi et al., 2011; Flaherty et al., 2010). Treatment with an anti-CTLA4 antibody can augment the anti-tumor immune response against melanoma tissue by blocking the immune-attenuating molecule, CTLA4, in T cells. However, the administration of the CTLA4 antagonist can induce severe autoimmune reactions, such as colitis and skin rashes (Weber, 2008). Therefore, it is essential to look for other therapeutic modalities with

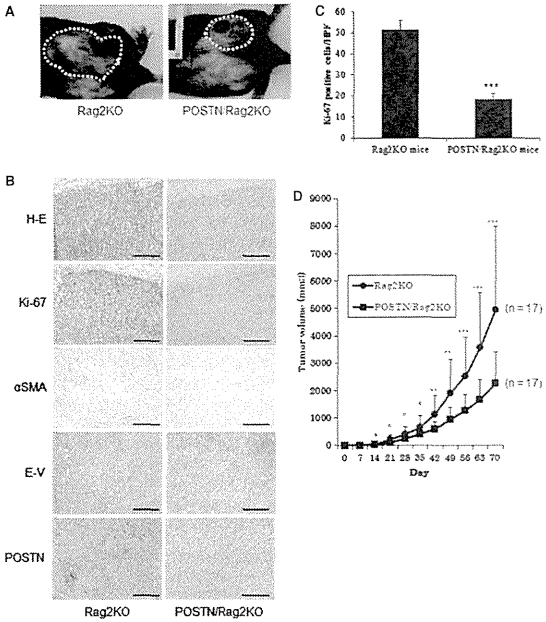

Figure 5. Melanoma tumorigenesis is significantly suppressed in *POSTN* gene knockout mice. Macroscopic feature of the *Rag2* KO and *POSTN/Rag2* KO mice on the day 56 after human melanoma cell implantation (A). There was decreased expression of Ki-67, αSMA, and collagen in the tumors of *POSTN/Rag2* KO mice. Dermal myofibroblast is positive for αSMA staining and collagen tissue becomes red by E-V (Elastica van Gieson) staining. Bar indicates 250 μm (B). There was a significant decrease in the number of Ki-67-positive cells in *POSTN/Rag2* KO mice (C). *There was significant suppression of* melanoma tumorigenesis in *POSTN* gene knockout mice (D). *, **, and *** indicate P-value <0.05, <0.01, <0.001, respectively.

novel mechanism(s) of action, which are not associated with such life-threatening adverse events. We believe that POSTN is important for the growth of melanoma, because the implanted melanoma cell grew more slowly in *POSTN*-depleted mice compared with matched control mice. A therapeutic approach targeting POSTN and its related signaling may lead to a safer treatment for malignant melanoma, and one that is less likely to be thwarted by resistance of the cancer cells.

In this experimental setting, there was no significant improvement in the overall survival in the POSTN-depleted mice even though the tumor growth was attenuated in KO mice compared with control mice on an immune-deficient background. There is no doubt that the survival is strongly dependent on the metastasis of the inoculated tumor cells, but we did not observe any metastasis in either the KO or wild-type mice, which likely contributed to the lack of a difference in the overall survival between the groups.

In conclusion, in human melanoma tissue, NHDFs interacted with melanoma cells to induce POSTN, which directly promoted melanoma cell proliferation by activating integrin/p44/42MAPK signals and indirectly instituted a fibrotic microenvironment in the tumor, thus resulting in a progression of the melanoma. As a result, the suppression of POSTN represents a novel therapeutic target for cutaneous malignant melanoma.

Methods

Cells and tissue samples

Human melanoma cell lines (MeWo, G-361, and VMRC-MELG) were obtained from the Japanese Collection of Research Bioresources (JCRB, Osaka, Japan), and NHDFs were obtained from TaKaRa Bio (Shiga, Japan). 293, 231, and A549 were represented by HEK293, MDA-MB-231, and A549 cancer cell lines loaded as positive controls, respectively (JCRB). All melanoma and normal tissue samples were obtained from patients at Osaka University Hospital (Department of Dermatology, Osaka, Japan). All clinical samples were collected after approval was obtained from the local ethics committee, and informed consent was obtained from each patient for use of the samples. Details of cell culture are described in Data S1.

Mice

Twelve-week-old Rag2-deficient (*Rag2*$^{-/-}$, C57BL/6 background) and periostin-deficient (*Postn*$^{-/-}$, C57BL/6 background) mice were used for the studies (Shimazaki et al., 2010). Experiments were undertaken following the guidelines for the care and use of experimental animals as required by the Japanese Association for Laboratory Animals Science (1987).

Sample preparation and iTRAQ labeling

Proteins were extracted from the frozen tumor and normal skin tissue samples. Details are described in Data S1.

Extracted proteins were purified using a 2D clean-up kit (GE Healthcare, Buckinghamshire, UK). Subsequently, 100 μg of each protein was dissolved, reduced, alkylated, and digested with trypsin, according to the manufacturer's protocol (Applied Biosystems, Foster City, CA, USA). The samples were labeled with iTRAQ reagent: reagent 114 for melanoma in situ, reagent 115 for normal skin lesions of melanoma in situ, reagent 116 for invasive melanoma, and reagent 117 for normal skin lesions of invasive melanoma. The labeled peptide samples were mixed and fractionated as described previously (Serada et al., 2010).

Mass spectrometric analysis and iTRAQ data analysis

NanoLC-MS/MS analyses and iTRAQ data analysis were performed as described in Data S1.

Western blot analysis

Cell lysates and supernatant fluids were used for the Western blot analyses. Details were described in Data S1.

Immunohistochemistry

Patient with paraffin-embedded melanoma tissue sections and in vivo mice melanoma tissue sections were stained with hematoxylin and eosin (H&E). For the immunohistochemical analysis, primary antibodies were used at the following dilutions: the human and mouse anti-POSTN (1:3000; Abcam, Tokyo, Japan), mouse anti-Ki-67 (1:500; Novocastra Laboratories Ltd, Newcastle, UK), and mouse anti-α-smooth muscle actin (α-SMA; 1:3000 dilution; Sigma-Aldrich, St. Louis, MO, USA). Details are described in Data S1.

Reverse transcription polymerase chain reaction (RT-PCR) analysis

To confirm the altered expression of POSTN in melanoma cells and NHDFs, melanoma cells (MeWo, G-361, and VMRC-MELG), NHDFs, and the cocultured cell samples were subjected to RT-PCR. β-actin was used as a housekeeping gene to evaluate and compare the quality of different cDNA samples. The primer sequences and the expected sizes of PCR products were as follows:

periostin, forward, 5′-TTGAGACGCTGGAAGGAAAT-3′
reverse, 5′-AGATCCGTGAAGGTGGTTTG-3′ (199 bp);
β-actin, forward, 5′-AGCCTCGCCTTTGCCGA-3′
reverse, 5′-CTGGTGCCTGGGGCG-3′(174 bp);

Details of total RNA extraction, quantitect reverse transcription, and RT-PCR are described in Data S1.

Quantitative reverse transcription polymerase chain reaction (qT-PCR) analysis

Normal human dermal fibroblasts were cocultured with CFSE-labeled MeWo and G-361 cells for 24 h. Thereafter, we sorted these cells into NHDF, MeWo, and G-361 cells using a FACS system. Next, the total RNA was isolated from the sorted NHDF, MeWo, and G-361 cells, and the products were reverse-transcribed into cDNA. The expression of TGFβ1, TGFβ3, IL-4, IL-13, BMP2, and PDGF-bb was measured using the Power SYBR Green PCR Master Mix (Applied Biosystems, Tokyo, Japan) according to the manufacturer's protocol. Glyceraldehyde-3-phosphate dehydrogenase (GAPDH) was used to normalize the mRNA, as GAPDH was not affected by the treatment. The primer sequences used were as follows:

TGFβ1, forward, 5′-TCGCCAGAGTGGTTATCTTTTG-3′
reverse, 5′-AGGAGCAGTGGGCGCTAAG-3′;
TGFβ3, forward, 5′-GCCCTTGCCCATACCTCCGC-3′
reverse, 5′-CGCAGCAAGGCGAGGCAGAT-3′;
GAPDH, forward, 5′-GGAGTCAACGGATTTGGTCGTA-3′
reverse, 5′-GCAACAATATCCACTTTACCAGAGTTAA-3′;
IL-4, forward, 5′-ACATTGTCACTGCAAATCGACACC-3′
reverse, 5′-TGTCTGTTACGGTCAACTCGGTGC-3′;
IL-13, forward, 5′-GCAATGGCAGCATGGTATGG-3′
reverse, 5′-AAGGAATTTTACCCCTCCCTAACC-3′;
BMP2, forward, 5′-ACTCGAAATTCCCCGTGACC-3′
reverse, 5′-CCACTTCCACCACGAATCCA-3′;
PDGF-bb, forward, 5′-CAGCGCCCATTTTTCATTCC-3′
reverse, 5′-GTTTTCTCTTTGCAGCGAGGC-3′.

Construction of a NHDF-derived POSTN expression vector

To construct a NHDF-derived POSTN expression vector, the cDNA of human POSTN derived from NHDFs cocultured with melanoma cells was amplified. The amplified cDNA was then inserted into the pcDNA3.1/V5-His-TOPO vector (Invitrogen, Carlsbad, CA, USA) and designated pcDNA3.1-POSTN.

Generation of NHDF-derived POSTN stable transfectant melanoma cells

To generate NHDF-derived POSTN stable transfectant cells (POSTN–MeWo), the MeWo cell line was transfected with pcDNA3.1-POSTN using Lipofectamine 2000 (Invitrogen) according to the manufacturer's instructions, after which the cells were selected with 500 μg/ml of Geneticin (GIBCO; Invitrogen). Stable clones were maintained in 250 μg/ml of Geneticin.

Proliferation assay

The proliferation of MeWo, G-361, VMRC-MELG, and POSTN–MeWo melanoma cells was examined using the Cell Counting Reagent SF (Nacalai Tesque, Kyoto, Japan) according to the manufacturer's recommendations, and then, absorbance was measured with a microplate reader (model 680; Bio-Rad, Tokyo, Japan) at test and reference wavelengths of 450 and 630 nm, respectively.

Kinase inhibition assays

The cells were incubated for 2 h with kinase inhibitors (Cell Signaling Technology, Beverly, MA, USA): LY294002 (10 μM) as an Akt inhibitor and PD98095 (10 μM) as a MAPK inhibitor. Cells were then stimulated with 100 ng/ml of recombinant POSTN in the same media. After stimulation, the MTT proliferation assay was performed.

Statistical analyses

The results are presented as the means ± SD. The analyses were carried out using the two-sided, unpaired Student's *t* test or the two-sided Welch test. Multiple comparisons between groups were made by Fisher's or Dunnett's methods. We considered values to be significant when $P < 0.05$.

Acknowledgements

This study was supported by a Grant-in-Aid for Young Scientists (B) (22791100) from the Japanese Ministry of Education, Science, Sports, and Culture; a Grant-in-Aid for the Program for Promotion of Fundamental Studies in Health Sciences of the National Institute of Biomedical Innovation; and a Grant-in-Aid from the Ministry of Health, Labour, and Welfare of Japan.

Disclosure statement

All authors declare no financial support or relationship that may pose conflict of interest.

References

Asano Y, I.H., Yamane K, J.M., Mimura, Y., and Tamaki, K. (2005). Increased expression of integrin alpha(v)beta3 contributes to the establishment of autocrine TGF-beta signaling in scleroderma fibroblasts. J. Immunol. *175*, 7708–7718.

Atefi, M., von Euw, E., Attar, N. et al. (2011). Reversing melanoma cross-resistance to BRAF and MEK inhibitors by co-targeting the AKT/mTOR pathway. PLoS ONE *6*, e28973.

Bao, S., Ouyang, G., Bai, X. et al. (2004). Periostin potently promotes metastatic growth of colon cancer by augmenting cell survival via the Akt/PKB pathway. Cancer Cell *5*, 329–339.

Baril, P., Gangeswaran, R., Mahon, P.C. et al. (2007). Periostin promotes invasiveness and resistance of pancreatic cancer cells to hypoxia-induced cell death: role of the beta4 integrin and the PI3k pathway. Oncogene *26*, 2082–2094.

Elliott, C.G., Wang, J., Guo, X. et al. (2012). Periostin modulates myofibroblast differentiation during full-thickness cutaneous wound repair. J. Cell Sci. *125*, 121–132.

Erkan, M., Kleeff, J., Gorbachevski, A. et al. (2007). Periostin creates a tumor-supportive microenvironment in the pancreas by sustaining fibrogenic stellate cell activity. Gastroenterology *132*, 1447–1464.

Flaherty, K.T., Puzanov, I., Kim, K.B. et al. (2010). Inhibition of mutated, activated BRAF in metastatic melanoma. N. Engl. J. Med. *363*, 809–819.

Gillan, L., Matei, D., Fishman, D.A., Gerbin, C.S., Karlan, B.Y., and Chang, D.D. (2002). Periostin secreted by epithelial ovarian carcinoma is a ligand for alpha(V)beta(3) and alpha(V)beta(5) integrins and promotes cell motility. Cancer Res. *62*, 5358–5364.

Guarino, M. (2010). Src signaling in cancer invasion. J. Cell. Physiol. *223*, 14–26.

Hanahan, D., and Weinberg, R.A. (2000). The hallmarks of cancer. Cell *100*, 57–70.

Horiuchi, K., Amizuka, N., Takeshita, S. et al. (1999). Identification and characterization of a novel protein, periostin, with restricted expression to periosteum and periodontal ligament and increased expression by transforming growth factor beta. J. Bone Miner. Res. *14*, 1239–1249.

Inai, K., Norris, R.A., Hoffman, S., Markwald, R.R., and Sugi, Y. (2008). BMP-2 induces cell migration and periostin expression during atrioventricular valvulogenesis. Dev. Biol. *315*, 383–396.

Kudo, Y., Ogawa, I., Kitajima, S. et al. (2006). Periostin promotes invasion and anchorage-independent growth in the metastatic process of head and neck cancer. Cancer Res. *66*, 6928–6935.

Li, J.S., Sun, G.W., Wei, X.Y., and Tang, W.H. (2002). Expression of periostin and its clinicopathological relevance in gastric cancer. World J. Gastroenterol. *13*, 5261–5266.

Li, G., Oparil, S., Sanders, J.M. et al. (2006). Phosphatidylinositol-3-kinase signaling mediates vascular smooth muscle cell expression of periostin in vivo and in vitro. Atherosclerosis *188*, 292–300.

Nyberg, P., Salo, T., and Kalluri, R. (2008). Tumor microenvironment and angiogenesis. Front Biosci. *13*, 6537–6553.

Ontsuka, K., Kotobuki, Y., Shiraishi, H. et al. (2012). Periostin, a matricellular protein, accelerates cutaneous wound repair by activating dermal fibroblasts. Exp. Dermatol. *21*, 331–336.

Ouyang, G., Liu, M., Ruan, K., Song, G., Mao, Y., and Bao, S. (2009). Upregulated expression of periostin by hypoxia in non-small-cell lung cancer cells promotes cell survival via the Akt/PKB pathway. Cancer Lett. *281*, 213–219.

Polyak, K., and Kalluri, R. (2010). The role of the microenvironment in mammary gland development and cancer. Cold Spring Harb. Perspect. Biol. *2*, a003244.

Puppin, C., Fabbro, D., Dima, M. et al. (2008). High periostin expression correlates with aggressiveness in papillary thyroid carcinomas. J. Endocrinol. *197*, 401–408.

Quaranta, V. (2002). Motility cues in the tumor microenvironment. Differentiation *70*, 590–598.

Riener, M.O., Fritzsche, F.R., Soll, C. et al. (2010). Expression of the extracellular matrix protein periostin in liver tumours and bile duct carcinomas. Histopathology *56*, 600–606.

Sasaki, H., Dai, M., Auclair, D. et al. (2001). Serum level of the periostin, a homologue of an insect cell adhesion molecule, as a prognostic marker in nonsmall cell lung carcinomas. Cancer *92*, 843–848.

Sasaki, H., Sato, Y., Kondo, S. et al. (2002). Expression of the periostin mRNA level in neuroblastoma. J. Pediatr. Surg. *37*, 1293–1297.

Sasaki, H., Yu, C.Y., Dai, M. et al. (2003). Elevated serum periostin levels in patients with bone metastases from breast but not lung cancer. Breast Cancer Res. Treat. *77*, 245–252.

Serada, S., Fujimoto, M., Ogata, A. et al. (2010). iTRAQ-based proteomic identification of leucine-rich alpha-2 glycoprotein as a novel inflammatory biomarker in autoimmune diseases. Ann. Rheum. Dis. *69*, 770–774.

Shao, R., Bao, S., Bai, X. et al. (2004). Acquired expression of periostin by human breast cancers promotes tumor angiogenesis through up-regulation of vascular endothelial growth factor receptor 2 expression. Mol. Cell. Biol. *24*, 3992–4003.

Shimazaki, M., Nakamura, K., Kii, I. et al. (2010). Periostin is essential for cardiac healing after acute myocardial infarction. J. Exp. Med. *205*, 295–303.

Soltermann, A., Ossola, R., Kilgus-Hawelski, S. et al. (2008a). N-glycoprotein profiling of lung adenocarcinoma pleural effusions by shotgun proteomics. Cancer *114*, 124–133.

Soltermann, A., Tischler, V., Arbogast, S. et al. (2008b). Prognostic significance of epithelial-mesenchymal and mesenchymal-epithelial transition protein expression in non-small cell lung cancer. Clin. Cancer Res. *14*, 7430–7437.

Takayama, G., Arima, K., Kanaji, T. et al. (2006). Periostin: a novel component of subepithelial fibrosis of bronchial asthma downstream of IL-4 and IL-13 signals. J. Allergy Clin. Immunol. *118*, 98–104.

Takeshita, S., Kikuno, R., Tezuka, K., and Amann, E. (1993). Osteoblast-specific factor 2: cloning of a putative bone adhesion protein with homology with the insect protein fasciclin I. Biochem. J. *294*(Pt 1), 271–278.

Tilman, G., Mattiussi, M., Brasseur, F., van Baren, N., and Decottignies, A. (2007). Human periostin gene expression in normal tissues, tumors and melanoma: evidences for periostin production by both stromal and melanoma cells. Mol. Cancer. *6*, 80.

Tischler, V., Fritzsche, F.R., Wild, P.J. et al. (2010). Periostin is up-regulated in high grade and high stage prostate cancer. BMC Cancer *10*, 273.

Weber, J. (2008). Overcoming immunologic tolerance to melanoma: targeting CTLA-4 with ipilimumab (MDX-010). Oncologist *13*(Suppl 4), 16–25.

Yan, W., and Shao, R. (2006). Transduction of a mesenchyme-specific gene periostin into 293T cells induces cell invasive activity through epithelial-mesenchymal transformation. J. Biol. Chem. *281*, 19700–19708.

Yang, C., Zeisberg, M., Lively, J.C., Nyberg, P., Afdhal, N., and Kalluri, R. (2003). Integrin alpha1beta1 and alpha2beta1 are the key regulators of hepatocarcinoma cell invasion across the fibrotic matrix microenvironment. Cancer Res. *63*, 8312–8317.